N 70 15166
NASA CR 107571

AN EXPERIMENTAL INVESTIGATION OF FLUCTUATIONS AND CORRELATIONS IN ELECTROMAGNETIC AND NUCLEAR SHOWERS DEVELOPING IN LEAD

by

Julius J. Brecht

Technical Report No. 955

March 1969

CASE FILE COPY

UNIVERSITY OF MARYLAND
DEPARTMENT OF PHYSICS AND ASTRONOMY
COLLEGE PARK, MARYLAND

Space Physics Group

This is a preprint of research carried out at the University of Maryland. In order to promote the active exchange of research results, individuals and groups at your institution are encouraged to send their preprints to

PREPRINT LIBRARY
DEPARTMENT OF PHYSICS AND ASTRONOMY
UNIVERSITY OF MARYLAND
COLLEGE PARK, MARYLAND
20742

U.S.A.

AN EXPERIMENTAL INVESTIGATION OF FLUCTUATIONS AND CORRELATIONS IN ELECTROMAGNETIC AND NUCLEAR SHOWERS DEVELOPING IN LEAD*

by

Julius J. Brecht

Technical Report No. 955

June 1969

Thesis submitted to the Faculty of the Graduate School
of the University of Maryland in partial fulfillment
of the requirements for the degree of
Master of Science
1969

*This research was supported by the National Aeronautics and Space Administration Grant NGR-21-002-066 and Grant ~~NGS-398~~. NGL-21-002-008

ABSTRACT

Title of Thesis: An Experimental Investigation of Fluctuations and Correlations in Electromagnetic and Nuclear Showers Developing in Lead

Julius J. Brecht, Master of Science, 1969

Thesis directed by: James A. Earl, Associate Professor of Physics

Electron showers at 105, 150, 300, 600, 1000, and 1200 MeV were studied using a Geiger tube hodoscope developed for balloon altitude observations of cosmic ray particles. The electron shower curves calculated from the experimental data are different from those obtained by other experimenters with various other detectors; the resulting computed track lengths are related to the incident electron energies by

$$\text{incident energy (MeV)} = (34.1 \pm 1.8) \times \text{track length (radiation lengths)}$$

as compared to

$$\text{incident energy (MeV)} = (17.1 \pm 1.4) \times \text{track length (radiation lengths)}$$

obtained with the detector's scintillation counter.

The percent fluctuation, f, in the track length based on scintillation counter pulse heights and corrected for intrinsic photoelectron statistics (proportional to one over the square root of the total number of events observed) was related to the incident electron

energy, E_o, in the energy interval 150 MeV $< E_o <$ 1200 MeV, by

$$f = (36\pm2)\left[\frac{E_o\ (\text{MeV})}{150\ \text{MeV}}\right]^{-(0.12\pm0.03)} \quad (\%)$$

The percent fluctuation in the track length based on Geiger tube discharge data in the energy region 105 MeV $< E_o <$ 1200 MeV decreased as the shower energy increased. The percent fluctuation in the number of shower particles was 74% Poisson in this energy interval and was a sizeable portion of the observed percent fluctuation for energies up to about 600 MeV. Beyond this energy, the percent fluctuations due to sampling dominated.

Extensive tables of the number of Geiger tube discharges were compiled. Correlations between the number of tubes discharged at two different depths were interpreted in terms of a model relating shower correlations to the total number of shower particles present and capable of discharging Geiger tubes and to the penetration probability of individual shower particles. This number varied with the incident electron energy as

$$\text{total number of electron shower particles} = (0.029\pm0.003)\text{x incident energy (MeV)}$$

The mean range, R, of the electron shower particles obtained from the penetration probability was

$$R = 0.9\pm0.4 \text{ radiation lengths}$$

which was consistent with that calculated as the ratio of the shower track length to the total number of shower particles based on Geiger tube discharge data.

Events obtained by exposing the detector to sea level cosmic ray mesons and to artificially accelerated protons and pions were treated in a manner identical to that used to analyze the electron data in hopes of detecting differences between electron showers and nuclear interacting events. Although some differences were found, the general characteristics of the nuclear interacting events were very similar to the electron showers.

ACKNOWLEDGMENTS

I wish to express my gratitude to Dr. James A. Earl for his patient and constructive supervision throughout the development of this thesis. I also acknowledge the encouragement offered me by my former advisor, Dr. Harold Zapolsky, and others in the department while I have attended the University of Maryland. I wish to thank Tom Rygg for the major computer programs and several interesting conversations.

Special recognition goes to my wife, Lucille, for her constant moral support in this endeavor.

Financial support of this research was provided by National Aeronautics and Space Administration Grant NGR-21-002-066, and computer time was made available by the National Aeronautics and Space Administration Grant NSG-398 to the Computer Science Center of the University of Maryland.

TABLE OF CONTENTS

LIST OF TABLES

FIGURE CAPTIONS

Figure 1 — Schematic diagram of the physical components of the detector. Particle trajectories selected by the directional filter coincidence requirements for trays 1 and 3 are indicated by dashed lines.

Figure 2 — Block diagram of detector electronics and monitoring equipment used in the experiment. There are ninety Geiger tubes and two scintillation counters in the detector.

Figure 3a,b,c — Typical oscilloscope monitor displays of a sea level cosmic ray meson event, a proton event, and an electron event measured by the detector. The first line in each display is a code to identify the event in a computer program. Lines 2 and 3 represent the dE/dx and calorimeter counter pulse heights in units of channels read 1 through 17 left to right. Dot number 9 is the same as dot number 10 in line 2 and in line 3. The dots in lines 4 through 8 are divided into two banks of 5x9. Each dot represents a Geiger tube in the hodoscope. The left and right banks represent the two stereoscopic views of a particle triggering the hodoscope, that is, line 6 corresponds to trays 5 and 6. A more intense dot implies a tube discharge.

Figure 4a,b — Schematic diagram of physical setup for exposure of the detector to 2GV and 4GV protons and pions using the Brookhaven Alternating Gradient Synchrotron and to high energy electrons using the Cornell electron synchrotron.

Figure 5 — Proton and pion calorimeter pulse height distributions for rigidities 2 GV and 4 GV and a sea level cosmic ray meson calorimeter pulse height distribution. The sea level cosmic ray meson distribution is composed of events having no multiple tube discharges in trays 5 through 10.

Figure 6 The dE/dx pulse height distributions for sea level cosmic ray meson events, for 2 GV and 4 GV clean proton events, and for electron showers. The experimental points for the electron shower distribution each represent an average over the data from the 105, 150, 300, 600, and 1200 MeV showers.

Figure 7 Calorimeter pulse height distributions for electron showers.

Figure 8 Track length percent fluctuations based on scintillation counter pulse heights, $\sigma_T/T = 28.8[(\Delta C_{obs})^2-(\frac{4}{3})C_o-C_s(\Delta C_o)^2]^{\frac{1}{2}}$, and based on observed Geiger tube discharges, $\sigma_T/T = 100\sigma_{n_{tot}}/\langle n_{tot}\rangle$, plotted as a function of electron shower energy for comparison. The points plotted are given in Table IV and Table VI.

Figure 9 Electron shower curves derived from Geiger tube information given in Table V and corrected for saturation using the model described in Chapter IV.

Figure 10 Track length percent fluctuations based on Geiger tube information plotted as a function of electron shower energy (same data as given in Figure 8). Also plotted are the track length percent fluctuations due to sampling uncertainties (denoted by the caption, "Var N_{tot} = 0"), $\sigma_T/T = [1/\langle n_{tot}\rangle - 1/\langle N_{tot}\rangle]^{1/2}$, and models for the percent fluctuation in the track length assuming the variance in the total number of particles in a shower is described by Poisson statistics (denoted by the caption "Var N_{tot} = $\langle N_{tot}\rangle$"), $\sigma_T/T = [1/\langle n_{tot}\rangle]^{1/2}$. The percent fluctuations in the track length based on Geiger tube data are fitted by a model assuming the percent fluctuations in the total number of particles in a shower is 74% Poisson (denoted by the caption, "Var N_{tot} = $0.6\langle N_{tot}\rangle$"), $\sigma_T/T = [1/\langle n_{tot}\rangle - .4/\langle N_{tot}\rangle]^{1/2}$.

Figure 11 1000 MeV electron shower curves obtained with the following detectors: scintillation counters, a multiplate cloud chamber, a lucite Cerenkov counter, a magnetic spark chamber, and a Geiger tube hodoscope. Also plotted are an Approximation B calculation with zero energy cutoff and a Monte Carlo calculation with a 10 MeV energy cutoff.

CHAPTER I

INTRODUCTION

Electromagnetic cascade showers produced by high energy electrons incident on high atomic number absorbers have been studied for many years. However, the rational design and evaluation of shower detecting instruments is still hampered by a lack of sufficiently detailed information about certain important shower characteristics. Since the National Aeronautics and Space Administration is about to undertake a major national research effort on high energy cosmic rays with an emphasis on definitive studies of cosmic electrons, this lack of information concerning shower characteristics will assume critical importance. One of the best ways of separating electrons from nucleons and of determining electron energies is by gathering detailed information on showers produced within a massive calorimeter.

This thesis deals with data obtained during calibration exposures of a Geiger tube hodoscope to artifically accelerated electrons, protons, and pions. The hodoscope had previously been used in many balloon borne experiments to gather data on primary cosmic radiation. The objective here is not only to calibrate a flight instrument but to attempt to present the data in a format applicable to instruments having various configurations. Although two scintillation counter pulse heights were obtained for each event, the basic information characterizing the development of the showers was the number of Geiger tube discharges in trays interspersed among lead plate absorbers. The response of a

detector embedded in absorbing material is critically dependent upon the nature of the detector. Consequently, the results given here differ significantly from those obtained with scintillation counters and other types of track forming detectors. It is hoped that the information presented will be useful in the design of specific detectors of similar configuration as well as in explaining some of the subtle issues of detector response which have caused the lack of information mentioned earlier.

A detailed study of correlations between the numbers of particles present at two different stages of shower development is undertaken. A simple statistical model has been devised relating these correlations to the mean range of the shower particles and to the total number of particles present in a shower. The model is used to obtain new estimates of these important parameters.

Various methods have been employed to study electron showers. Kantz and Hofstadter (1953) observed showers in copper using sodium iodide crystals and photomultiplier tubes and later extended their study to carbon, aluminum, tin, and lead (Kantz and Hofstadter, 1954). Crannell (1967) used the same method in a thorough investigation of shower energy deposition. Blocker, Kenney, and Panofsky (1950) used an ionization chamber to study electron showers in carbon, aluminum, copper, and lead. Scintillation plastic counters with photomultiplier tubes have been used by Backenstoss, Hyams, Knop, and Stierlin (1963), by Beuermann and Wibberenz (1967), and by Neely (1968). Murata (1965) used X-ray photographic films of different sensitivities to observe both the longitudinal

and lateral development of showers in lead. A similar investigation was conducted by Jenkins, Cobb, Nelson, and McCall (1965) and later by Nelson, Jenkins, McCall, and Cobb (1966) using the thermoluminescent properties of lithium-fluoride crystals.

In addition to the above total energy deposition measurments, electron showers have been studied by Cronin, Engels, Pyka, and Roth (1962) using lead plates and a spark chamber and by Kajikawa (1963) using a glass-lead plate spark chamber. Lengeler, Deutschmann, and Tejessy (1963) have investigated electron shower characteristics with a propane bubble chamber. Becklin and Earl (1964) and Thom (1964) used multiplate cloud chambers while Heusch and Prescott (1964) worked with a lucite Cerenkov counter. Most recently, a magnetic spark chamber has been used by Drickey, Kilner, and Benaksas (1968) to observe the charged component of 1-GeV electron showers in lead.

Several mathematical models have been put forth to describe electron shower development in high-Z materials. Rossi and Greisen (1941) proposed an analytical method to describe the longitudinal development of electron showers - Approximation B - involving a lower limit for shower particle energies. Wilson (1952) postulated an analytical model based on a Monte Carlo calculation that could generate a particle shower with specified characteristics - incident energy, shower particle trajectory, and minimum shower particle energy. This approach was later improved upon by Belen 'kii and Ivanenko (1959) and Butcher and Messel (1960). These methods were refined by Messel, Smirnov, Varfolomeev, Crawford, and Butcher (1962) and by Crawford and Messel (1962) to include a variety of

interactions and to give the radial, as well as, longitudinal development of electron showers in lead and emulsions. Nagel (1965) has also used the Monte Carlo method to provide theoretical shower curves in lead for several incident electron and photon energies down to a 1.5 MeV cutoff energy.

The literature indicates that the Monte Carlo calculations agree in general with experimental data from detectors with high energy cutoffs.

This thesis is divided into three basic parts: a description of the experimental equipment and setup, analysis of the data, and conclusions. Included in the development of the first division is a description of the detector (Chapter II), the procedure used to calibrate the scintillation counters using minimally ionizing singly charged particles, and the experimental setup for obtaining the electron shower data (Chapter III).

A model is presented to relate the number of tubes discharged at a given depth to the number of shower particles incident and capable of discharging a Geiger tube (Chapter IV). Shower curves obtained using this relation are given as a function of energy. The data obtained from the scintillation counters and Geiger tubes is used to calculate electron shower track lengths and other related parameters. In addition, the fluctuation in track lengths based on scintillation counter pulse heights and Geiger tube information is investigated and the fluctuations in Geiger tube discharges are studied as a function of shower energy and depth. Comparisons are made between these results and the literature when possible.

The correlation between the average number of Geiger tubes discharged at a depth X_A and those discharged at depth X_B ($X_A<X_B$) in several centimeters of lead is investigated for electron showers and proton and sea level cosmic ray meson events measured by the detector (Chapter V). The correlation data are of intrinsic interest in the study of electron showers. In addition, a model using these data is presented that might be useful in distinguishing electrons from protons in cosmic ray beams.

Conclusions are summarized in Chapter VI.

CHAPTER II

THE DETECTOR

The physical components of the detector —— the hodoscope, the dE/dx and calorimeter counters —— are described. The directional filter coincidence requirements and general detector information are also presented. Related data monitoring equipment is discussed along with general procedures for data acquisition and reduction.

A. Components

The detector is a hodoscope consisting of layers of lead, scintillation counters, and Geiger tubes as shown in Figure 1. Incident electrons produce showers in lead plates of approximately 1 r.l. thickness (5.83 gm/cm^2 = 1X_o). Sheets of plastic scintillator 0.0177 r.l. thick are placed near lead plates to sample the development of the showers and are divided into two counters, each of which is connected to a separate pulse height analyzer. The dE/dx counter consists of a single plate located in the incident beam of particles before they enter the lead plates. Its function is to measure the ionization rate of incident particles. The calorimeter counter is made up of five plates located between lead slabs in the detector. Its function is to sample the total energy loss of particles contained in the shower. A directional filter coincidence requirement (to be explained later) is imposed on incident particles. The detector is

9.31 r.l. thick (8.16 r.l. lead).

1. Hodoscope. The hodoscope detectors serving to define particle trajectories are organically quenched Geiger tubes 14.2 cm long and 1.58cm in diameter.These tubes are arranged in trays of nine with the tube axes of trays 1,3,5,7,9 perpendicular to those of 2,4,6,8,10. Since all tubes have separate analysis circuits, one obtains essentially stereoscopic views of particle trajectories through the detector.

A block diagram of the detector and monitor electronics setup is given in Figure 2. Each Geiger tube is connected to a binary circuit. Suppose one or more tubes are discharged somewhere in tray 1 through tray 10. A fraction of a microsecond later, the discharge pulses flip the corresponding tube binary circuits. Shortly afterwards, if the trigger signal depicted in Figure 2 indicates that the incident phenomena are acceptable, it causes a hold signal to be sent from the control electronics circuit to the tube binaries. This signal converts the binaries from monostable to bistable modes and gates off all further inputs. At the same time, it causes shift pulses to be sent into the tube binaries making the binaries act as shift registers. The hold signal changes the binary mode from event detection to event readout and is kept on until three readouts of the data are performed. In later data analysis, these readouts are compared to detect and to prevent errors due to lost or erroneous bits. If there is no trigger signal, then the binaries automatically reset after 5μsec. If one now

imagines all of the Geiger tube binaries in their shift mode, then the discharged tube information will pass through the tube and counter binaries (to be explained later) to a control electronics circuit where it is read out to a tape recorder or other monitoring units.

2. dE/dx and calorimeter counters. The dE/dx counter is connected via a light pipe to a photomultiplier tube and is used to determine if an incident particle was minimally ionizing. It is situated above tray 3. The output of its photomultiplier is pulse shaped to be acceptable to the first of two pulse height analyzer amplifiers having gains of 10 each shown in Figure 2. Together, the two span a factor of 100 in pulse height, or energy loss, over 17 channels using ladder attenuators. Each step of attenuation is associated with a channel and has its own binary circuit. Therefore, each channel represents a factor of 4/3 in pulse height. The information in the attenuator binaries is shifted along with that from the Geiger tubes for each acceptable event. Table I gives the conversion between pulse height and channel number. The analyzer channels in this table range from 0 to 8 in 0.1 intervals.

The five calorimeter counter plastic scintillator slabs are all connected via light pipes to a single photomultiplier tube whose pulse height analyzer circuits are the same as those for the dE/dx counter. Calorimeter data from acceptable events are read out along with that from the Geiger tubes and the dE/dx counter. The calorimeter counter detects the total ionization of all particles emerging from the lead plates which is proportional to the total energy dissipated

in these plates by shower particles.

A lead plate 0.98 r.l. thick is situated underneath tray 10 to insure that its response to backscattering particles is the same as the other trays.

3. Directional filter coincidence requirements. The directional filter coincidence requirements are specified to select incident particle trajectories so that the resulting showers do not develop through one of the sides of the detector. Physically, four-fold coincidences of tube discharges in the top four trays of the hodoscope are required. The allowed sequences of tube discharges for trays 1 and 3 are connected by dashed lines in Figure 1. The corresponding sequences for trays 2 and 4 are similar. These criteria select incident particle trajectories less than about 20° off the detector axis. The directional filter spacing (distance between trays 1 and 3 or 2 and 4) was 7.35cm.

Other selection criteria were imposed in the computer data analysis.

4. General detector information The detector is 33 cm in height and weighs about 100 pounds exclusive of power supply. It has a dead time/event of 430 msec (circulation/readout time). Two Deltron 6v power supplies were used to run the detector. A precision 1kHz tuning fork oscillator was used to drive the detector electronics.

B. Data

The data were collected on magnetic tapes in an analog format along with a reference time in the laboratory. The latter provided a basis for comparison of calibration phenomena with changes in the beam characteristics. An Ampex Model 220 audio tape recorder, depicted in Figure 2, was used with four track 1/4 inch magnetic tapes.

The data were also continuously monitored on a cathode ray oscilloscope programmed to display Geiger tube discharges as particles passed through the detector. A photograph of three typical series of discharges seen on this apparatus are shown in Figure 3a, b, c and represent, respectively, a sea level cosmic ray meson, a proton event containing anuclear interaction in a lower tray, and an electron shower. The first line in each is an identification code which simplifies the task of finding events using the computer. Lines 2 and 3 are the dE/dx and calorimeter counter pulse heights in channels read 1 through 17 left to right. The discriminator levels of the last stage of the first pulse height analyzer amplifier and the first stage of the second are the same, so dot number 9 is the same as dot number 10 in line 2 and in line 3. The dots in line 4 through 8 are divided into two banks of 5 x 9. Each dot represents a Geiger tube in the hodoscope. The left and right banks represent the two stereoscopic views of a particle triggering the hodoscope, that is, line 6 corresponds to trays 5 and 6. A more intense dot implies a tube discharge. This apparatus was also of particular use in checking the response of the instrument

to sea level meson events — an important calibration procedure.

The data were later translated from analog to digital form using the facilities at the Goddard Space Flight Center in Greenbelt, Maryland. The digital tapes were further reduced using the IBM 7094 computer at the Computer Science Center of the University of Maryland.

The selection criterion imposed on the computerized data was the following: that one and only one Geiger tube be discharged per directional filter tray. This requirement eliminated interactions occurring in the directional filter trays. Only one incident particle was to be analyzed by the hodoscope at a time. In addition to this criterion, the data were also analyzed by separating them into events containing no nuclear interactions and those that developed showers.

CHAPTER III

EXPERIMENTAL CONFIGURATION AND CALIBRATION

The total average pulse height from the calorimeter counter is proportional to the total track length of the particle or particles passing through the counter as will be shown later. The shower electrons are minimally ionizing, so both the dE/dx and calorimeter counters must be calibrated with singly charged minimally ionizing particles. The effect of possible nuclear interactions on the counter pulse heights produced by the incident calibrating particle must be deleted to obtain the total pulse height due only to the incident particle. A study of the detector's response to sea level cosmic ray mesons (noninteracting particles) and to electrons was also carried out.

An incident particle passing through a lead plate in the detector may suffer ionization, radiation, or nuclear interaction energy losses. For electrons of several hundred million electron volts energy, radiation losses are by far greater than the other two. The photons created by this energy loss may undergo pair production or Compton scattering and, in turn, produce electrons of about the same energy as the initiating photon. These secondary electrons may then experience radiation losses. The net result of this cyclic process is a cascade shower. The number of shower particles increases until the

average energy of the electrons created is low enough for collisional losses to play a dominant role, and the shower dies. Scintillator plastic slabs are placed next to the lead plates to detect the emerging shower particles which may interact with the scintillator atoms and give information on the number of particles passing through the calorimeter counter and their total energy loss.

An electron shower is represented by the oscilloscope monitor display of tube discharges in the detector given in Figure 3c. The incident electron passes through the first two lead plates (see detector physical schematic, Figure 1) without causing multiple tube discharges in a tray. However, in passing through the next plate, it develops a shower and causes two tube discharges in tray 7, and four discharges in tray 8. The shower develops further in passing through lead plate 5 and causes multiple tube discharges in trays 9 and 10. This incident electron had an intial ionization loss rate of 5 channels and a total energy loss rate in the region of the calorimeter of 9 channels. The Geiger tube discharges detect the lateral spread and longitudinal development of the shower.

A. Response to Protons and Pions

The calibration was performed at the Brookhaven National Laboratories, Alternating Gradient Synchrotron. Although this synchrotron had the capacity to accelerate protons to 28GeV, the detector was placed in a parasitic beam with two momentum analyzing magnets capable of yielding particles of maximum rigidity 4GV. This beam was

produced by allowing the main beam to strike a target giving off a variety of particles as shown in Figure 4a.

Calibration runs were made at 2 and 4GV with and without a lead shield in front of the detector, and the rigidity was defined within $\pm$ 1%. The beam was pulsed every 2 sec, and a gating circuit allowed the hodoscope to trigger for 50msec. To avoid confusion, the detector was permitted to trigger on only one event per acceleration beam pulse. The major components of the main beam are protons and pions with a small amount of positrons resulting from pion decays $\pi^{+} \rightarrow \mu^{+} \rightarrow e^{+}$ (Fitch, Meyer, Piroue´, 1962). The positrons were eliminated from the beam on some calibration runs by placing a slab of lead 3 r.l. thick in front of the detector so that the positrons would develop showers before reaching the detector.

Table II gives the total number of Geiger tube discharges observed as a function of incident energy for 2 and 4GV protons. Also given are the total number of events observed and the percent and number of events satisfying the directional filter selection criterion - one and only one discharge per tray in the first four Geiger tube trays. There were 7330 proton events accepted out of 8332 detected. Consequently, the number of events was sufficient for adequate statistical accuracy in the distribution of pulse heights. Also listed in Table II are the corresponding data for sea level cosmic ray mesons and electron showers to be discussed in later sections.

A computer scanning program was used to further reduce the proton data by separating the events into those containing no nuclear interactions and those that contain at least one nuclear interaction.

The particles given off in a nuclear interaction may discharge more than one Geiger tube in a given tray. The occurrence of a nuclear interaction was defined in this program by the presence of three or more tube discharges in one of trays 5 through 10 or by two or more discharges in at least two of these trays. Such events will hence forth be referred to as dirty proton events. A graph of the resulting calorimeter pulse height distribution for the dirty proton events is given in Figure 5 (solid line curve) as well as for proton events having no nuclear interactions as defined by the absence of multiple tube discharges (dashed line curve). These latter events will be referred to as clean proton events.

There is a possiblity that several particles in a nuclear interaction go through one Geiger tube. Such interactions would go undetected by the criterion described above. However, these interactions would broaden the calorimeter pulse height distribution for events supposedly containing no nuclear interactions. To determine the amount of these residual interactions, the calorimeter distributions at 2 GV and 4 GV were compared with that of sea level cosmic ray mesons which are an excellent example of noninteracting penetrating particles. The latter's distribution is also plotted in Figure 5. Its shape and size are identical to the clean proton event distribution within experimental error. This result indicates the contribution of residual interactions in this proton distribution, undetected by the computer scanning program, was less than experimental error. The relatively

large number of events in calorimeter channel 0 represents all events whose pulse heights are not large enough to enter channel 1.

The standard deviation of the clean proton event and meson distributions is 1.6 channels as opposed to 3.0 channels for the dirty proton event distribution. Table III gives the average pulse heights and standard deviations for the dE/dx and calorimeter counters for the proton experiments and sea level cosmic ray mesons. Comparison of the combined calibration runs with the lead shield in place at 2GV and 4GV with the combined runs at 2 GV and 4 GV without lead implies the effect of positrons in the beam is small. The combination of 2 and 4GV calibration runs with no lead shield in front of the detector was used in further reducing the data.

The average pulse height for minimally ionizing, singly charged, clean particle events was 3.05 ± 0.03 channels. Other pulse heights will be expressed relative to this one using Table I.

The above analysis of the calorimeter pulse height distributions assumed that the incident particles were all minimally ionizing. This assumption can be checked by comparing the respective dE/dx pulse height distributions given in Figure 6. The sea level cosmic ray meson, 2GV and 4GV proton event distributions are of approximately the same size and shape although the meson distribution peak is slightly lower than that of the protons. Also plotted are the distributions for electron showers to be discussed in the next section.

B. Electron Exposure

The facilities of the Cornell University Electron Synchrotron were used to obtain dE/dx and calorimeter pulse heights of showers produced in lead by electrons of known energy. The incident electrons were the result of pair production by Bremsstrahlung gamma rays striking a lead target. The emerging beam was momentum analyzed before passing on to the detector.

The experimental arrangement used is given in Figure 4b. Measurements were taken at 105, 150, 300, 600, 1000, and 1200 MeV by varying the current of the analyzing magnet. The detector was inclined at 10° to the beam during the 1000 MeV exposure, however, all the other experiments were conducted with the incident electron trajectory parallel to the detector axis. The rigidity was defined to within ±7% at 1GV. The synchrotron was pulsed every 1/60 sec providing the detector with a few electrons per second.

Table II shows that several thousand showers were observed at each energy. Consequently, the number of events was sufficient for adequate statistical accuracy in the distribution of pulse heights.

Figure 7 gives the pulse height distribution for the calorimeter counter for the incident electron energies investigated. The higher the incident electron's energy, the larger the average pulse height for the resulting shower. The average pulse heights and standard deviations for the dE/dx and calorimeter counters are given in Table III as a function of incident electron energy. The resolution of the counters

will be discussed in detail in Chapter IV. Table III also gives the standard errors (standard deviation/square root of the total number of events) in the dE/dx and calorimeter pulse heights.

Since the ionization energy loss rate is essentially constant over the incident electron energies studied ($\beta \sim 1$), the individual dE/dx distributions all lay on top of one another within experimental error. These data were averaged to give the electron dE/dx distribution in Figure 6. It has the same shape and size as that for the sea level cosmic ray mesons, 2GV and 4GV proton events. These observations show that very few events were produced by multiple incident particles.

CHAPTER IV

ELECTRON SHOWER TRACK LENGTHS AND FLUCTUATIONS

An important parameter of an electron shower is its track length defined as the integral under the curve of average number of particles plotted as a function of depth. It is a measure of the total distance traveled by all particles in the shower in units of radiation lengths. Track lengths were computed from the observed scintillation counter pulse height data and from the observed Geiger tube shower curves. A comprehensive comparison of these results and those from various other experimental and theoretical (Monte Carlo calculations) methods of determining track lengths is presented in this chapter. The observed track lengths based on scintillation counter pulse heights were in agreement with those presented in the literature; however, the observed track lengths based on Geiger tube shower curves were perceptibly different from other experimentally determined track lengths. The shower curves obtained from the Geiger tube information were decidedly different from the other experimentally and theoretically determined curves.

It is commonly assumed in the literature that the electron shower energy, E_o, is directly proportional to the track length, T,

$$E_o = \varepsilon T \qquad \text{(IV-1)}$$

where ε is the constant of proportionality measured in units of MeV/r.l. and is called the track length constant. Values of the track length constant are computed from the observed data and compared with values given in the literature. In general, the track length constant increases as the shower energy increases for the observed scintillator pulse height and Geiger tube data implying the rate of energy dissipation is not independent of shower energy. The average values of the track length constant calculated from the scintillation counter pulse height data and from the Geiger tube data in the energy range 105 MeV $< E_o <$ 1200 MeV were respectively, 17.2±1.4 MeV/r.l. and 34.1 ± 1.8 MeV/r.l. The logarithmic slopes, κ, of the shower curves at large depths, defined as d ℓn N/dx, are also computed from the observed Geiger tube data and compared to those values given in the literature. The variance in these observed track lengths was investigated, and a graph of track length fluctuations as a function of shower energy is plotted for the scintillation counter pulse height data and Geiger tube data.

The dependence of the variance in the number of Geiger tubes discharged in a tray on depth is considered and compared with values quoted in the literature. It was found that the variance dependence on depth is quite different from that observed in other experiments.

A. Track Lengths Based on Scintillation Counter Pulse Heights

Track lengths, T, were computed from the observed data by numerical integration of the shower curves:

$$T = \sum_k N_k \Delta X_k \qquad \text{(IV-2)}$$

where N_k is the number of particles present at depth X_k, and ΔX_k is the width of the interval over which N_k is measured. For the observed scintillation counter pulse height data, ΔX_k, was a constant equal to 1.43r.1. The summation, $\sum_k N_k$, is then just the ratio of the average shower pulse height to the average pulse height for a minimally ionizing singly charged particle (clean proton event). However, a correction must be made for the portion of the shower that develops beyond the calorimeter counter. For the energies studied here, the shower curves have constant exponential decay factors at depths corresponding to the last few scintillator plastic slabs. Hence, the portion of the track length not measured by the calorimeter counter can be approximated by N_L/κ. Here, N_L is the number of particles detected by the last scintillator and κ is the logarithmic slope of the extrapolated shower curve. The data of Neely (1968) were used for these calculations.

The resulting track lengths and track length constants, ε, obtained from the scintillation counter data are listed in Table VII under the heading "Observed-Scintillation Counter." Also tabulated are other values for track length, shower curve exponential slope, and track length constant in the literature which will be discussed later. The error due to differing sensitivities of the five scintillator plastic slabs of the

calorimeter counter was found to be negligible. The main source of error in these track lengths stems from the normalization of the shower average pulse heights by that of a clean proton event pulse height and amounts to about ±0.2 channels. As the incident electron energy decreases, the track length of the shower decreases.

The variance in the track length, T, based on scintillation counter pulse heights was also investigated. Since the track length is directly proportional to the electron shower average pulse height, P_s, one has

$$\frac{\sigma_T}{T} = \frac{\Delta P_s}{P_s} \qquad \text{(IV - 3)}$$

where σ_T and ΔP_s are the respective standard deviations of T and P_s. The standard deviation of P_s in units of pulse height may be obtained from the standard deviation of the shower average pulse height in channels. These latter standard deviations are listed in Table III and range from 1.16 ± .02 channels at 1200 MeV to 2.01 ± .03 channels at 105 MeV.

The relationship between channels, C, and pulse height, P, for a scintillation counter pulse height distribution was discussed in Chapter II and is

$$P = (4/3)^G \qquad \text{(IV-4)}$$

Therefore, taking the natural logarithm of both sides of (IV-4) and allowing P and C to fluctuate by respective amounts ΔP and ΔC results in a percent fluctuation of the scintillation counter pulse height distribution given by

$$\frac{\Delta P}{P} = 28.8\Delta C \qquad \text{(IV-5)}$$

The observed percent fluctuationsin the electron shower average pulse height, $\Delta P_{os}/P_{os}$, at a given energy are composed of an intrinsic fluctuation due to photoelectron statistics in the counters, $\Delta P_i/P_i$, and a shower fluctuation, $\Delta P_s/P_s$:

$$\frac{\Delta P_{os}}{P_{os}} = 100 \left[\left(\frac{\Delta P_i}{P_i} \right)^2 + \left(\frac{\Delta P_s}{P_s} \right)^2 \right]^{1/2} \qquad \text{(IV - 6)}$$

Using (IV-5), the percent fluctuation in the average pulse height, P_o, of one clean proton event may be expressed in terms of the fluctuations of the average pulse height in units of channels, ΔC_o,

$$\frac{\Delta P_o}{P_o} = 28.8\ \Delta C_o \qquad \text{(IV - 7)}$$

The percent fluctuation due to N such particles would then be 28.8 ΔC, where ΔC is

$$\Delta C = \frac{1}{\sqrt{N}} \Delta C_o \qquad \text{(IV - 8)}$$

In the case of electron showers observed with a scintillation counter, the value used for N is

$$N_s = P_s/P_o \qquad \text{(IV - 9)}$$

Combining (IV-4, 5, 8, 9), $\Delta P_i/P_i$ becomes

$$\frac{\Delta P_i}{P_i} = 28.8\ (\tfrac{4}{3})^{(C_o-C_s)/2}\ \Delta C_o \qquad \text{(IV - 10)}$$

where C_o and C_s are the respective average pulse heights of the clean proton event and electron shower in units of channels. Therefore, substituting (IV-10) into (IV-6), using $\Delta P_{os}/P_{os} = 28.8\ \Delta C_{os}$, and (IV-3), the percent fluctuation in the electron shower track length is

$$\frac{\sigma_T}{T} = 28.8\ [(\Delta C_{os})^2 - (\tfrac{4}{3})^{C_o-C_s}(\Delta C_o)^2]^{1/2} \qquad \text{(IV - 11)}$$

Table IV lists the percent fluctuation due to photoelectron statistics, $\Delta P_i/P_i$, given by (IV-10) and the percent fluctuation in shower track length, σ_T/T, given by (IV-11) as a function of shower energy. The percent fluctuation due to the photoelectron statistics increases as the shower energy decreases. The 300MeV electron shower scintillation counter pulse height distribution had the same observed percent fluctuation (46%) as that of the pulse height distribution of a clean proton event. A graph of (IV-11) plotted against the incident

electron energy, E_o, for the showers investigated is given in Figure 8. A solid line curve is fitted to these points. This percent fluctuation, σ_T/T, may be expressed as a power law of the incident electron energy,

$$\frac{\sigma_T}{T} = (36 \pm 2) \left[\frac{E_o(\text{MeV})}{150\ \text{MeV}}\right]^{-(0.12 \pm 0.03)} \qquad \text{(IV - 12)}$$

in the energy interval 150 MeV$<E_o<$1200 MeV. Below 150 MeV, the percent fluctuations drop off sharply. In this region, a large protion of the shown particles have barely enough energy to reach the first scintillator slab of the calorimeter counter. These particles end up depositing only enough energy in the counter's scintillator slabs to register in the zero channel of the electron shower pulse height distribution and should not be considered as contributing to the percent fluctuations in the track length based on scintillation counter pulse heights. However, this effect cannot be separated from that produced by events that pass through all five scintillator slabs of the calorimeter counter and register an energy loss corresponding to the zero channel of the shower pulse height distribution.

B. Track Lengths Based on Geiger Tube Information

The Geiger tube data related to electron shower curves are in terms of average number of tubes discharged per tray. To obtain a track length based on this information, a model relating the average number of tubes discharged per tray and the average number of particles present at the tray is needed.

1. Geiger tube shower curve data. The Geiger tube discharge data from various experiments were preserved in their entirety at the time of data taking. Later a computer scanning program deleted any events in which more than one tube was discharged in any directional filter tray thus discriminating against interactions and multiple incident particles. Table II gives the total number of Geiger tube discharges observed as a function of incident electron energy along with the total number of events observed, percent and number of events used in further data analysis. There were enough tube discharges to provide adequate statistical accuracy.

Various parameters may be calculated from the Geiger tube information. In particular, matrices of the number of times tubes in a given tray were discharged were compiled as a

function of incident electron energy. From this format, the average number of tubes discharged in the i^{th}/tray, $\langle n_i \rangle$, was calculated and the results are given in Table V along with the variance, σ_i^2, in the number of tubes discharged in the i^{th} tray as a function of energy and depth in the shower. Values for $\langle n_i \rangle$ were computed using the summation

$$\langle n_i \rangle = \sum_{j=1}^{9} P_{ij}\, j \qquad \text{(IV - 13)}$$

where P_{ij} is the probability of having j discharges in the i^{th}/tray or the ratio of the number of discharges in the i^{th}/ tray to the total number of showers used.

2. Relationship between tubes discharged and particles present. If the number of shower particles, N_A, per unit area passing through a plane at a depth X_A perpendicular to the longitudinal development of the shower is small enough, then the probability, P_A, of more than one particle passing through a given tube would be negligible. Hence, the average number of tube discharges at X_A would be equal to the average number of particles present and capable of discharging a Geiger tube. As the incident electron energy increases, however, N_A also increases possibly becoming large enough to make P_A signigicant, and the capability of the Gieger tubes to distinguish individual particles as single tube

discharges diminishes. The hodoscope is said to saturate under these conditions.

To correct for the saturation effect, the following model was devised: assume that exactly N particles are incident on the Geiger tubes of a tray in the hodoscope. Let ρ_k be the probability that a given particle passes through the k^{th}/ tube in the tray. Then $\sigma_k = 1-\rho_k$ is the probability that it does not pass through the k^{th}/tube. Assuming that the particles are statistically independent, the probability that the k^{th}/ tube is discharged with N particles incident is

$$p_k(N) = 1-\sigma_k^N \qquad \text{(IV - 14)}$$

The average number of tubes discharged in a tray for N particles incident is then

$$\langle n \rangle_N = \sum_{k=1}^{9} (1-\sigma_k^N) \qquad \text{(IV - 15)}$$

Expanding (IV-14) in a power series gives

$$\begin{aligned} \langle n \rangle_N &= \sum_k 1-[1-N\rho_k + \frac{N(N-1)}{2!}\rho_k^2 + \ldots] \\ &= N\,[1- \frac{N-1}{2!} \sum_k \rho_k{}^2 + \ldots] \end{aligned} \qquad \text{(IV - 16)}$$

Note that

$$\sum_{k=1}^{9} \rho_k = 1 \qquad \text{(IV - 17)}$$

Let $P_n(N)$ be the probability that n tubes are discharged when N particles are incident on a tray, and let P_N be the probability that N particles are incident on that tray. Then the average number of tubes discharged for an average number of particles incident, $\langle N \rangle$, is

$$\begin{aligned} \langle n \rangle_{\langle N \rangle} &= \sum_{N} \sum_{n} P_N n \, P_n(N) = \sum_{N} P_N \langle n \rangle_N \\ &= \sum_{N} P_N N \left[1 - \frac{N-1}{2!} \sum_{k} \rho_k^2 + \ldots\right] \end{aligned} \qquad \text{(IV - 18)}$$

Let

$$\alpha \equiv \frac{1}{2!} \sum_{k=1}^{9} \rho_k^2 \qquad \text{(IV - 19)}$$

Then (IV - 18) becomes

$$\langle n \rangle_{\langle N \rangle} \simeq (1 + \alpha)\langle N \rangle - \alpha \langle N^2 \rangle \qquad \text{(IV - 20)}$$

Let p_A be the probability that a particle is incident on tray A, and let q_A be the probability that a particle is not incident on that tray. Then the probability, P_{N_A}, that after η independent trials, N_A particles

are incident on tray A is given by the binomial formula

$$P_{N_A} = \frac{\eta!}{N_A!\ (\eta - N_A)!}\ p_A^{N_A}\ q^{\eta - N_A} \qquad \text{(IV - 21)}$$

The expectation values in (IV - 20) may be evaluated using (IV - 21) and the binomial distribution generating function, G,

$$G^{\eta} = (p_A s + q)^{\eta} \qquad \text{(IV - 22)}$$

The resulting average number of tube discharges in tray A when an average number of particles, $\langle N_A \rangle$, are incident is

$$\langle n_A \rangle_{\langle N_A \rangle} = \langle N_A \rangle\ (1 - \alpha \langle N_A \rangle) \qquad \text{(IV - 23)}$$

assuming $\eta >> 1$.

The Geiger tube and scintillation counter data were compared to obtain a numerical value for the saturation effect constant, α. If the summation in (IV - 18) is extended over all tubes in trays 5 through 10, then the corresponding first order approximation for the average total number of tubes discharged is $\langle n_{tot} \rangle_{N_{obs}}$,

$$\langle n_{tot} \rangle_{N_{obs}} = N_{obs}\ (1 - \alpha'\ N_{obs}) \qquad \text{(IV - 24)}$$

where

$$\alpha' = \frac{1}{2!} \sum_{k=1}^{54} \rho_k^2 = 6\alpha \qquad \text{(IV - 25)}$$

The total average number of shower particles incident on and capable of discharging the Geiger tubes in trays 5 though 10 is represented by N_{obs}. However, N_{obs} is unknown at this point, so the normalized average pulse height given by (IV - 9) is used in its place. By plotting $\langle n_{tot} \rangle N_{obs}/6(\frac{Ps}{Po})$ against $(\frac{Ps}{Po})$ and correcting for the relative responses of Geiger tubes and scintillation plastic, the saturation effect constant, α, was found to be

$$\alpha = 0.087 \pm 0.009 \qquad \text{(IV - 26)}$$

Assume ρ_k is equal to $1/\nu$, where ν is the number of tubes involved per tray - those tubes discharged most often on the average for all showers. Then using (IV - 19) for the saturation effect constant leads to $\alpha = 1/2\nu$. Substituting (IV - 26) for the saturation effect constant results in $\nu = 6 \pm 1$ tubes. Hence, one would expect the lateral width of the showers to be about 6 tubes. This conclusion is confirmed by the computer shower data. Since the average number of tube discharges per tray, $\langle n \rangle$, is at most about 3 discharges/tray, it is not unreasonable that the probability of more than one particle passing through a given tube per shower is small.

The shower curves based on scintillation counter pulse height data of Neely (1968) were also used to check the magnitude of the saturation effect constant. The result was $\alpha = 0.076 \pm 0.006$ which is consistent with the value given in (IV - 26).

Using the saturation effect constant, α, defined by (IV - 26), (IV - 23) may be rearranged to give

$$\langle N_A \rangle \simeq \langle n_A \rangle \langle N_A \rangle \left(1+\alpha \langle n_A \rangle \langle N_A \rangle\right) \qquad \text{(IV - 27)}$$

The shower curves shown in Figure 9 were computed using (IV -26) and (IV - 27) for the energies investigated. The result of the saturation effect correction is to shift the entire Geiger tube shower curve of tube discharges up - more so near shower maximum than anywhere else.

3. Track lengths. The track lengths based on Geiger tube data were computed by numerical integration of the Geiger tube shower curves using (IV - 2). Values of N_k were calculated using (IV - 27), and the quantity ΔX_k was a constant equal to 1.49 r.l. However, a correction was made for that portion of the shower that developed beyond the hodoscope. At the energies studied here, the shower curves have constant exponential decay factors at depths corresponding to the latter trays in the detector. Hence, as in the case of track lengths based on scintillation counter pulse heights, the portion of the track length not measured by the hodoscope was analytically determined.

The resulting observed and extrapolated track length based on Geiger tube data and corrected for the saturation effect are listed in Table VII under the heading "Observed - Geiger Tube." The main sources of error here are due to the uncertainty in the saturation effect constant, α, and in the logarithmic slope ($\kappa = d\ln\langle N\rangle/dx$); both are included in the corresponding track length errors. Also given are the logarithmic slopes of the shower curves at large depths under the heading "Slope" and the track length constant, ε.

The variance in the track lengths based on the Geiger tube information was investigated as a function of energy. This track length is directly proportional to the average total number of Geiger tubes discharged, $\langle n_{tot}\rangle$, in the electron shower. The percent fluctuation in the track length, σ_T/T is then

$$\frac{\sigma_T}{T} = 100\ \frac{\sigma_{n_{tot}}}{\langle n_{tot}\rangle} \qquad \text{(IV - 28)}$$

where σ_T and $\sigma_{n_{tot}}$ are the respective standard deviations in track length and total number of tubes discharged. Numerical values for $\langle n_{tot}\rangle$ and $\sigma_{n_{tot}}$ were obtained from the Geiger tube data using a computer program.

Table VI gives the resulting values of σ_T/T, $\langle n_{tot}\rangle$, and $\sigma_{n_{tot}}$. In general, $\langle n_{tot}\rangle$ and $\sigma_{n_{tot}}$ decrease as the incident electron energy

decreases ranging, respectively, from 14.23±0.22 tube discharges and 3.06±0.06 tube discharges at 1200 MeV to 2.57±0.06 tube discharges and 1.53±0.03 tube discharges at 105 MeV. A plot of the track length percent fluctuations given by (IV - 28) as a function of the incident electron energy, E_o, is shown in Figure 10. These percent fluctuations gradually increase more rapidly as the energy decreases.

The following model was devised to explain this behavior: the average total number of tube discharges, $\langle n_{tot} \rangle$, may be related to the average total number of shower particles, $\langle N_{tot} \rangle$, capable of discharging Geiger tubes by

$$\langle n_{tot} \rangle = \sum_{n_{tot}, N_{tot}} n_{tot} P_{n_{tot}}(N_{tot}) \, P_{N_{tot}} = \sum_{N_{tot}} p \, N_{tot} P_{N_{tot}}$$

$$= p \langle N_{tot} \rangle \qquad \text{(IV - 29)}$$

Here, $P_{n_{tot}}(N_{tot})$, is the probability of having n_{tot} tubes discharged when N_{tot} particles are in the shower, and $P_{N_{tot}}$ is the probability that N_{tot} particles are present. It has been assumed that the total average number of tubes discharged, $\langle n_{tot} \rangle_{N_{tot}}$, when N_{tot} particles are in a shower is directly proportional to the total number of particles, N_{tot}, where the constant of proportionality is p. Similarly, the variance in the total number of tubes discharged is given by

$$\text{Var } n_{tot} = \sum_{n_{tot},N_{tot}} n_{tot}^2 P_{n_{tot}}(N_{tot})\, P_{N_{tot}} - \langle n_{tot} \rangle^2 \qquad \text{(IV - 30)}$$

Graphs of the probability distribution of the total number of tubes discharged were plotted and fitted to normal distribution functions - a limiting case of the binomial distribution. Using the latter distribution function, the variance becomes

$$\text{Var } n_{tot} = p(1 - p)\, N_{tot} = \langle n_{tot}^2 \rangle - \langle n_{tot} \rangle^2 \qquad \text{(IV - 31)}$$

Substituting (IV - 31) into (IV - 30), dividing by the square of (IV - 19), taking the square root of this fraction, and multiplying by 100 gives the percent fluctuation in the track length, σ_T/T,

$$\frac{\sigma_T}{T} = \frac{[\text{Var } n_{tot}]^{1/2}}{\langle n_{tot} \rangle} = 100 \left[\frac{1-p}{p} \frac{1}{\langle N_{tot} \rangle} + \frac{\text{Var } N_{tot}}{\langle N_{tot} \rangle^2} \right]^{1/2} \qquad \text{(IV - 32)}$$

The first term in (IV - 32) , $(1-p)/p\langle N_{tot} \rangle$, considers fluctuations due to sampling statistics, and the second term, $\text{Var}N_{tot}/\langle N_{tot} \rangle^2$, considers fluctuations due to uncertainties in the number of shower particles present.

Consider the case where the number of shower particles does not fluctuate, then (IV - 32) reduces to

$$\left.\frac{\sigma_T}{T}\right|_S = 100\left[\frac{1}{\langle n_{tot}\rangle} - \frac{1}{\langle N_{tot}\rangle}\right]^{1/2} \qquad \text{(IV - 33)}$$

using (IV - 29). Values of the total number of shower particles capable of discharging Geiger tubes are given in Table VIII and will be used here deferring discussion of the method of obtaining them to Chapter V. The percent fluctuations due to sampling given by (IV - 33) are plotted in Figure 10 and denoted by the caption, "Var N_{tot} = 0." The error bars are based on errors in the total number of shower particles. The percent fluctuations due to sampling decrease rapidly as the energy increases in the energy range 105MeV<E_o<300MeV and is a constant (19%) in the interval 300MeV<E_o<1200MeV. The entire curve lies below the Geiger tube data. The difference between the experimental percent fluctuations using (IV - 28) and the percent fluctuations due to sampling using (IV - 33) is interpreted as the result of intrinsic fluctuations in the number of shower particles present and capable of discharging Geiger tubes.

For example, assume that the fluctuations in the number of these particles is described by a Poisson distribution, then Var N_{tot} = $\langle N_{tot}\rangle$, and (IV - 32) becomes

$$\left.\frac{\sigma_T}{T}\right|_P = 100\left[\frac{1}{\langle n_{tot}\rangle}\right]^{1/2} \qquad \text{(IV - 34)}$$

These percent fluctuations are also plotted in Figure 10 as a function of incident electron energy and denoted by the caption, "Var $N_{tot}=\langle N_{tot}\rangle$." This curve lies entirely above the Geiger tube data and generally decreases as the energy increases. Hence, (IV - 32) with Var $N_{tot} = Q\langle N_{tot}\rangle$, where $0<Q<1$, might be expected to fit the percent fluctuations in track length based on Geiger tube information,

$$\frac{\sigma_T}{T} = 100 \left[\frac{1-p}{p} \frac{1}{\langle N_{tot} \rangle} + \frac{Q}{\langle N_{tot} \rangle} \right]^{1/2} \qquad \text{(IV - 35)}$$

The experimental points were fitted by the solid line in Figure 10 calculated using (IV - 35) with $Q=0.6$. This result implies the percent fluctuations in the total number of shower particles was 74% Poisson.

Comparison of the observed track length percent fluctuations, (IV - 28), with that using (IV - 34) shows that for energies in the region $105\text{MeV}<E_o<600\text{MeV}$, the intrinsic percent fluctuations in the number of shower particles is a sizeable portion of the observed percent fluctuations. The implication here is that any improvement in the sampling statistics would not change the observed percent fluctuations in the track length appreciably. However, at higher energies, the observed percent fluctuations become almost entirely due to sampling and could be decreased by increasing the number of Geiger tube trays used to measure the electron shower over a given depth interval.

Figure 8 displays the fluctuations based on scintillation counter pulse heights and based on Geiger tube data for comparison. The Geiger tube data are approximated by a dashed line. At lower energies (105MeV< E_o <150MeV), the two types of detectors have vastly different percent fluctuation dependences on incident electron energy. But after the two curves cross at 300 MeV, they appear to approach a constant negative slope of about -0.12.

C. Intercomparison of Track Lengths Derived by Various Methods

Table VII includes values of track lengths, shower curve logarithmic slope, and track length constant, ε, reported by Becklin and Earl (1964), and Thom (1964) using multiplate cloud chambers; Neely (1968), Beuermann and Wibberenz (1967), and Backenstoss, Hyams, Knop, and Stierlin (1962) using scintillation counters; Heusch and Prescott (1964) using a lucite Cerenkov counter; Drickey, Kilner, and Benaksas (1968) using a magnetic spark chamber; Kajikawa (1963), and Cronin, Engels, Pyka, and Roth (1962) using a spark chamber; and Lengeler, Deutschmann, and Tejessy (1963) using a propane bubble chamber. Some of the shower parameters were not given in several of these references. When possible, values of track length, shower curve logarithmic slope past shower maximum, and track length constant were approximated from data given in the references and are followed in the table by an iden-

tifying asterisk. In addition, a Monte Carlo calculation by Crawford and Messel (1962) for several electron energies is given for an energy cutoff of 10 MeV.

The observed track length and track length constant based on the scintillation counter pulse height distributions are in agreement with those of Neely as would be expected since his values of shower curve logarithmic slope past shower maximum were used in obtaining the total shower track lengths. Beuermann and Wibberenz's value for 200 MeV showers and 440 MeV showers for the track length constant is higher than the observed value calculated for a 600 MeV electron shower.

The observed track lengths based on Geiger tube information are consistently smaller than those of other types of detectors over the energy range investigated. The Monte Carlo calculations by Crawford and Messel for electron shower track length agree with the track lengths based on Geiger tube discharge information although their respective shower curves over the observed energy range are decidedly different.

Figure 11 displays shower curves obtained at a standard energy of 1000 MeV with various detectors including the multiplate cloud chamber, lucite Cerenkov counters, magnetic spark chamber, scintillation counter, and the hodoscope (using (IV - 25) and (IV - 26)). These experimental results are compared with Monte Carlo calculations by

Messel, Smirnov, Valfolomeev, Crawford, and Butcher (1962) with a 10MeV energy cutoff and an Approximation B calculation (Rossi and Greisen, 1941) for a zero energy cutoff (Snyder, 1938). The shower curves of the other detectors are quite different from that of the hodoscope. The hodoscope curve has a lower shower maximum and less steep slope at large depths than the shower curves of the other detectors. The multiplate cloud chamber, lucite Cerenkov counter, and magnetic spark chamber have high energy cutoffs for charged particles, and in the case of electrons, respond mainly to those having an energy above 10MeV. Neely's scintillation counter was reported to have a cutoff energy of approximately 8 to 10 MeV.

The hodoscope appears to measure more particles than the other detectors at large depths except for the scintillation counters of Neely. This effect may be due to the fact that the Geiger tubes are capable of detecting particles in the shower that are below the sensitive range of the other detectors. The various detectors discussed have different responses to different particles. For example, the multiplate cloud chamber only responds to shower electrons above a certain energy such that the electron tracks are distinguishable on a photographic film. The Cerenkov counter is sensitive only to electrons of sufficient energy to produce Cerenkov light, and the scintillation counter is sensitive to both electrons and gamma rays. The hodoscope, however, is composed of Geiger tubes that are sensitive to both electrons and photons down to very low energies - the particle must have enough energy to pass through 0.06 r.l. of Geiger tube wall.

The Monte Carlo calculation shower curves were devised for high energy electrons and photons and agree in general with the shower curves obtained with cloud chambers, Cerenkov counters, spark chambers, and magnetic spark chambers. In contrast, the hodoscope shower curves are decidedly different from these curves.

Comparison of the shower curve based on Geiger tube data with Snyder's calculation using Approximation B for a zero energy cutoff shows that the theoretical curve is consistently far about the curve based on Geiger tube data and has a different shape.

D. Fluctuations

The dependence of the variance in tube discharges on shower depth is also of interest. Table V gives the variance (σ^2) of tubes discharged per tray as a function of depth and shower energy. These variances were calculated from the computer matrices mentioned in section B of this chapter.

$$\sigma^2 = \langle n^2 \rangle - \langle n \rangle^2 \qquad \text{(IV - 28)}$$

A graph of variance in number of tube discharges per tray plotted as a function of depth in the shower is given in Figure 12 for the hodoscope at a standard energy of 1000 MeV. Similar curves are plotted for various other detectors: a lucite Cerenkov counter (Heusch and Prescott, 1964), scintillation counters (Neely, 1968), and a multiplate cloud chamber

(Thom, 1964). These experimental results are compared with a Monte Carlo calculation (Messel, Smirnov, Varfolomeev, Crawford, and Butcher, 1962) having an energy cutoff of 10MeV. The variance curve based on Geiger tube data is perceptibly less steep past the variance maximum than the curves based on the other detector data. The observed variance curve is clearly less steep past variance maximum than the Monte Carlo calculation curve.

CHAPTER V

CORRELATIONS

The correlation coefficient, $\rho(N_A,N_B)$, between the number of particles, N_A and N_B, at two depths, X_A and X_B, in an electron shower is defined as

$$\rho(N_A,N_B) = \frac{C(N_A,N_B)}{[\ \text{Var}\ N_A\ \ \text{Var}\ N_B\ ]^{1/2}} \qquad (V - 1)$$

The covariance in the number of particles at depths X_A,X_B is represented by $C(N_A,N_B)$, and the variances in the number of particles at depth X_A and at depth X_B are represented, respectively, by $\text{Var}\ N_A$ and $\text{Var}\ N_B$. These functions are defined as

$$C(N_A,N_B) = \langle N_A N_B \rangle - \langle N_A \rangle \langle N_B \rangle \qquad (V - 2)$$

and

$$\text{Var}\ N_A = \sigma^2_{N_A} = \langle N_A^2 \rangle - \langle N_A \rangle^2 \qquad (V - 3)$$

The standard deviation of the number of particles at depth X_A is represented by σ_{N_A}. The covariance in tube discharges offers another parameter to investigate electron showers.

Values of the correlation coefficient and covariance were calculated in terms of Geiger tube discharges using a computer program and (V - 1,2,3). These data were obtained for the fifteen pairs of trays (see Figure 1): 5-6, 5-7,···, 5-10, 6-7,···, 6-10, 7-8,···,7-10, 8-9, 8-10, 9-10 for electron showers at 105, 150, 300, 600, 1000, and 1200 MeV and for proton and sea level cosmic ray meson events. The dependence of the covariance in the number of tube discharges on tray separation, $X_B - X_A$, in units of radiation lengths is given in graphical form.

A model is presented to relate the covariance in the number of particles incident on and capable of discharging Geiger tubes to the covariance in the number of tubes discharged and to the total average number of particles in the showers as a function of incident electron energy. The average number of electron shower particles ranged from 36.5±6.5 at 1200 MeV to 4.0±0.7 at 105 MeV and are tabulated. A modified form of the model is applied to the proton and sea level cosmic ray meson data, and the resulting average numbers of shower particles are listed.

Probability distributions for Geiger tube discharges were calculated for each of the trays for the electron showers and for the proton and sea level cosmic ray meson events studied. Binomial probability distributions were fitted to the tube discharge distributions using the above mentioned values of total number of shower particles at a given incident electron energy. Poisson probability distributions were also calculated for each tray using the average number of tubes discharged in a tray as the mean of the distribution. In general, these two distributions approximated the tube discharge data of trays 6 through 10 over three decades of

probability (0.001 to 1.0) for the electron showers but not for the proton or sea level cosmic ray meson events.

The electron showers are also studied from the standpoint of penetration probability. This quantity is defined as the probability that a particle present at depth, x, has penetrated from a depth, x-t. A model is devised to express the penetration probability in terms of Geiger tube information (covariance in the number of tube discharges and average number of tubes discharged per tray). The model is modified to investigate proton and sea level cosmic ray meson events. A graph of penetration probability as a function of tray separation is presented for the electron showers and proton events.

The mean range, R, of electron shower particles may be defined as

$$R = T/N \qquad (V - 4)$$

where T represents the track length of the N particles in the shower. Another method of determining the mean range is developed based on the shape of the curve of penetration probability as a function of tray separation. These two methods both give an electron shower particle mean range of about 0.9±0.4 r.l. over the energy region studied.

Proton and sea level cosmic ray meson event mean ranges were also calculated using the above two methods assuming the protons and mesons were electron-like particles. The resulting mean range for 2 GV and 4GV protons was about 1.8±0.2 r.l. The sea level cosmic ray meson mean range was 1.5±0.7 r.l. although the meson data may be contaminated with

electrons. The results of these calculations are listed.

The derived information on electron showers and proton events is useful in the design of detectors and might lead to a method of separating electrons from protons and other particles in a cosmic ray beam.

A. Covariance As a Function of Depth

The covariance in the number of tube discharges for electron showers is presented. A model is devised to relate the covariance in the number of particles incident on and capable of discharging Geiger tubes to the covariance in the number of Geiger tube discharges. The number of particles in a shower is then obtained using this relationship. The probability distribution of the tube discharges in each of trays 5 through 10 is investigated as a function of energy.

1. Covariance in the number of Geiger tube discharges for electron showers. The covariance in the number of Geiger tube discharges for the various combinations of trays was computed using (V - 2), and the resulting data are plotted as a function of depth in radiation lengths in Figure 13. The data in general are approximated by the smooth line shown. At small tray separations, the covariance is relatively large and decreases as the separation increases. At large separations, the covariance becomes negative and approaches a constant value. A representative error bar is given on the graph. The different tray separations in the hodoscope span a range of 1.38 r.l. to 7.65 r.l. The dispersion in the covariance data at a given tray separation does not appear to be dependent on the shower

energy and is most likely due to statistical uncertainties in the data.

2. Relationship between covariance in the number of Geiger tube discharges and the covariance in the number of shower particles. Two typical trays, A and B, situated below the directional filter trays of the hodoscope and separated by a lead plate are represented in Figure 14. Particle trajectories in a shower are represented as straight lines tipped with arrows indicating the particles' directions of motion. A line through a circle, representing a Geiger tube, corresponds to a tube discharge. The incident particles may be divided into three groups: those created before tray A and absorbed between trays A and B, those created between trays A and B and absorbed beyond tray B, and those created before tray A and absorbed beyond tray B. Let these three classifications be denoted by the letters A, B, and C respectively.

The number of particles, N(x), present at depth, x, may be related to the probability, P(x-t,t), that a particle created at depth, x-t, will be present at depth, x,

$$N(x) = \int_0^\infty n(x-t)\ P(x-t,t)\ dt \qquad (V - 5)$$

The number of particles created in the interval, x-t, is given by n(x-t). The shower electrons undergo radiation energy losses. This loss mechanism is dependent upon the electronic charge of the containment medium and the energy of the electron. Therefore, assume that the survival probability, P(x-t,t), is independent of longitudinal position in the

hodoscope,

$$P(x-t,t) = P(t) \qquad (V - 6)$$

The average number of penetrating particles, $N_C(x_C)$, originating before tray A and absorbed beyond tray B would then be expressed in terms of the survival probability, $P_B(t)$,

$$\langle N_C \rangle = \langle N_B \rangle - \int_{x_A}^{x_B} n(x-t)\ P_B(t)\ dt \qquad (V - 7)$$

where n(x-t) represents the number of particles produced between trays A and B and capable of reaching tray B. The average number of particles passing through tray B is represented by $\langle N_B \rangle$.

One wishes to find the covariance between particles passing through tray A and through tray B. The class of penetrating particles, C, is a subset of the class of particles passing through tray A and the class of particles passing through tray B. Let the respective probabilities of a given particle falling into these categories be p_A, p_B, p_C, and let the probability of the incident particle satisfying none of these classifications be p_D. Assuming N independent trials, the joint probability of having N_A particles passing through tray A and N_B particles passing through tray B is given by the multinomial distribution function, M,

$$M = \frac{N!}{N_A!N_B!N_C!N_D!}\ p_A^{N_A}\ p_B^{N_B}\ p_C^{N_C}\ p_D^{N_D} \qquad (V - 8)$$

Using this distribution function, the covariance, $C(N_A,N_B)$, in the number of particles, N_A and N_B, present at trays A and B is given by

$$C(N_A,N_B) = \sum_{N_A,N_B,N_C} (N_A+N_C)(N_B+N_C)M - \langle N_A+N_C\rangle\langle N_B+N_C\rangle \qquad (V - 9)$$

By making use of the generating function, G, for the multinomial distribution,

$$G^N = (p_A s + p_B t + p_C u + q)^N \qquad (V - 10)$$

one obtains

$$C(N_A,N_B) = - \frac{\langle N_A\rangle\langle N_B\rangle}{N} + \langle N_C\rangle \qquad (V - 11)$$

The first term in (V - 11) considers particles passing through tray A and not tray B or passing through tray B and not tray A. The second term in (V - 11), $\langle N_C\rangle$, represents the covariance contribution due to penetrating particles passing through both tray A and tray B. The quantity, N, represents the total number of particles in the shower capable of discharging Geiger tubes.

The covariance, $C(n_A,n_B)$, in tube discharges in trays A and B may be written using the definition (V - 2),

$$C(n_A,n_B) = \sum_{n_A,n_B} n_A n_B\, p(n_A,N_A)\, p(n_B,N_B)\, P(N_A,N_B) - \langle n_A\rangle\langle n_B\rangle \qquad (V - 12)$$

where $P(N_A,N_B)$ is the joint probability of having N_A particles at depth, x_A, and N_B particles at depth, x_B, and is given by the multinomial distribution in (V - 8). The conversion factors, $p(n_A,N_A)$ and $p(n_B,N_B)$, from number of tubes discharged to number of particles present for trays A and B may be obtained using (IV - 15) assuming the saturation effect constant $\alpha<<1$. For example,

$$n_A[p(n_A,N_A)] = [1 - \alpha(N_A - 1)]N_A \qquad (V - 13)$$

Combining (V - 11) and (V - 12) gives

$$C(n_A,n_B) = C(N_A,N_B) - \alpha[\, C(N_A^2,N_B) + C(N_A,N_B^2)\,] \qquad (V - 14)$$

The saturation effect term, $\alpha[\, C(N_A{}^2,N_B) + C(N_A,N_B{}^2)\,]$, may be expressed in terms of the particle covariance, $C(N_A,N_B)$, using (V - 10) and an operator equation. Remembering that the class of penetrating particles, C, is a subset of the class of particles passing through tray A and the class of particles passing through tray B, one has

$$C(N_A^2,N_B) = \left(s\frac{\partial}{\partial s} + u\frac{\partial}{\partial u}\right)^2 \left(t\frac{\partial}{\partial t} + u\frac{\partial}{\partial u}\right) G^N \Big|_{s,t,u=1}$$

$$C(N_A,N_B^2) = \left(s\frac{\partial}{\partial s} + u\frac{\partial}{\partial u}\right) \left(t\frac{\partial}{\partial t} + u\frac{\partial}{\partial u}\right)^2 G^N \Big|_{s,t,u=1} \qquad (V - 15)$$

Summing the results of (V - 15) and combining them with (V - 14) gives

$$C(n_A,n_B) = C(N_A,N_B)\ [\ 1 - 2\alpha(\langle n_A\rangle + \langle n_B\rangle)\ ] \qquad (V - 16)$$

Assuming the saturation constant $\alpha<<1$, (V - 16) may be rearranged to give

$$C(N_A,N_B) = C(n_A,n_B)\ [\ 1 + 2\alpha(\langle n_A\rangle + \langle n_B\rangle)\ ] \qquad (V - 17)$$

The term, $2\alpha(\langle n_A\rangle + \langle n_B\rangle)$, accounts for the saturation effect on the particle covariance.

The covariance in number of particles given by (V - 16) may be used in conjunction with (V - 11) to obtain the average number of shower particles based on Geiger tube information. For large tray separations, the effect of penetrating particles on the particle covariance is negligible. Then (V - 11) would reduce to

$$C(N_A,N_B) \simeq -\frac{\langle N_A\rangle\langle N_B\rangle}{N} \qquad (V - 18)$$

In order to determine how large the separation must be to ensure the accuracy of (V - 18), the covariance in the number of particles, corrected for saturation, given in (V - 17) was plotted as a function of tray separation for each shower energy. The range where the covariance is a more or less constant negative value may then be determined. It is this region where (V - 18) is valid. The corresponding covariances may be

used with (V - 18) to obtain the average number of shower particles based on Geiger tube information. The resulting numbers are given in Table VIII and range from 36.5±6.5 at 1200 MeV to 4.0±0.7 at 105 MeV.

Figure 15 displays the total number of shower particles as a function of shower energy. The number of shower particles rises slowly as the shower energy increases in the region of 105MeV to 300 MeV and then increases linearly with the shower energy. The total number of shower particles, N, in the energy range 105MeV<E<1200 MeV may be related to the incident electron energy, E, by

$$N = (0.029 \pm 0.003) E(\text{MeV}) \qquad (V - 19)$$

The distribution of Geiger tube discharges in each of trays 5 through 10 was investigated for the electron showers and the resulting experimental probabilities are given in Table IX for the energies studied. Binomial probability distributions were calculated assuming the probability of a tube discharge was given by the ratio of the average number of tube discharges in a tray (see Table V) to the average total number of particles in the shower (see Table VIII). This method neglects the second order saturation effect. A Poisson probability distribution was also calculated for each experimental distribution using the average number of tubes discharged as the distribution mean. The two theoretical distributions approximated the experimental distribution points over a wide range of probability (0.001 to 1.0) for trays 6 through 10 in the energy range from 105 MeV to 1200 MeV. The theoretical probability distribution

curves did not fit the experimental data for tray 5. The experimental probability distributions exhibited a much lower probability of having zero tube discharges and a much higher probability of having one tube discharge compared to the theoretical curves. This effect became more pronounced the higher the shower energy. An incident high energy electron has passed through about 5.7 gm/cm^2 of lead in getting to tray 5, and its chances of being absorbed beyond tray 5 are good. Therefore, the probability of its not discharging a Geiger tube in tray 5 would be small and its probability of discharging just one tube would be large.

A representative set of probability distributions is given in Figure 16 for tray 7. The solid points correspond to a 600 MeV electron shower at shower maximum. The solid line curve corresponds to a binomial distribution with a probability of having a tube discharge of 0.131 and a value of 16 for the total number of shower particles. The dashed line corresponds to a Poisson distribution with a mean of 2.09 tubes discharged. The theoretical curves fit the experimental points equally well over a wide range.

The distribution of Geiger tube discharges in each of trays 5 through 10 was also investigated for 2 GV and 4 GV dirty proton events and for sea level cosmic ray meson events. The latter events were satisfied by the same tube discharge criteria as the dirty proton events. The resulting experimental probability distributions of tube discharges for electron showers at shower maximum were not distinguishable from the corresponding proton or sea level cosmic ray meson event tube discharge distributions at the same depth.

B. Penetration Probability

A model relating the penetration probability to the covariance in the number of Geiger tube discharges and the corresponding average number of tube discharges is presented for electron showers. The model is also applied to protons and sea level cosmic ray meson events treated as electron showers.

1. Electron showers. Points, x, on an electron shower curve may be roughly approximated by a straight line of positive slope before shower maximum and negative slope after shower maximum,

$$n(x-t) = n_B \left[1 \pm |\kappa| (x - x_B) \right] \qquad (V - 20)$$

Here, κ, is the logarithmic slope of the shower curve divided by the number of particles, n_B, created in an interval dt between trays A and B. The plus and minus signs in front of κ are used, respectively, after and before shower maximum. The parameter, κ, may be written as

$$\kappa = \frac{n_A - n_B}{n_B(x_B - x_A)} \equiv \frac{\beta}{x_B - x_A} \qquad (V - 21)$$

Combining (V - 7, 20, 21) results in

$$\langle N_C \rangle = \langle N_B \rangle - \int_0^{\Delta x} n_B (1 \pm \kappa t) \, P_B(t) \, dt \qquad (V - 22)$$

where Δx is the separation between trays A and B. Similarly, the aver-

age number of particles passing through tray B is

$$\langle N_B \rangle = \int_0^\infty n_B(1 \pm \kappa t) P_B(t)\, dt \qquad (V - 23)$$

The ratio of $\langle N_C \rangle$ to $\langle N_B \rangle$ may then be obtained,

$$\frac{\langle N_C \rangle}{\langle N_B \rangle} = 1 - \frac{\int_0^{\Delta x} (1 \pm \kappa t) P(t)\, dt}{\int_0^\infty (1 \pm \kappa t) P(t)\, dt} \qquad (V - 24)$$

Two different relations were used for the survival probability, P(t), to investigate its dependence on the shower curve logarithmic slope,

$$P_1(t) = \begin{cases} 1 & 0<t<R \\ 0 & \text{elsewhere} \end{cases} \qquad (V - 25)$$

and

$$P_2(t) = e^{-t/R} \qquad (V - 26)$$

The quantity, R, defines the mean range of the particles involved. The ratio, $\langle N_C \rangle / \langle N_B \rangle$, was calculated for several different values of β defined by (V - 21) using (V - 24, 25, 26) and found to be relatively independent of the shower curve exponential slope. The quantity, $\langle N_C \rangle / \langle N_B \rangle$, will then be interpreted as the probability that a particle present at tray B has penetrated from tray A and will be referred to as a penetration probability. Combining (V - 11) and (V - 16), solving for the average number of penetrating particles, $\langle N_C \rangle$, and dividing by $\langle N_B \rangle$ results in

$$\frac{\langle N_C \rangle}{\langle N_B \rangle} = \frac{\langle N_A \rangle}{N} + \frac{C(n_A, n_B)}{\langle N_B \rangle} \left[1 + 2\alpha(\langle n_A \rangle + \langle n_B \rangle) \right] \qquad (V - 27)$$

or in terms of Geiger tube discharges

$$\frac{\langle N_C \rangle}{\langle N_B \rangle} = \frac{\langle n_A \rangle (1+\alpha\langle n_A \rangle)}{N} + \frac{C(n_A, n_B)}{\langle n_B \rangle} \frac{\left[1 + 2\alpha(\langle n_A \rangle + \langle n_B \rangle) \right]}{1 + \alpha\langle n_B \rangle} \qquad (V - 28)$$

A graph of penetration probability defined by (V - 28) is plotted as a function of tray separation, $X_B - X_A$, in Figure 17 for the electron shower energies investigated. The data is approximated by a smooth curve. As the tray separation, $\Delta X = X_B - X_A$, goes to zero, the numerator of the fraction in (V - 24) goes to zero, and the probability that a particle present at tray B has penetrated from tray A goes to one. Hence, the zero depth penetration probability is plotted at 1.0. The penetration probability is a sharply decreasing function of tray separation for depths less than 1 r.l. and approaches zero more gradually at larger depths.

Various tray combinations (see Figure 1) are indicated in Figure 17 next to the respective calculated penetration probabilities. The mean depths of tray combinations 5-6, 7-8, and 8-9 are about 2 r.l., 5 r.l., and 6 r.l., respectively. However, these three combinations each have a tray separation of about 1.4 r.l. Examination of the relative penetration probabilities shows the observed dispersion in probabilities is not dependent on depth in the shower. Also note that the dispersion in

penetration probabilites at a given tray separation is not dependent on the shower energy.

The dispersion in the points at 1.4 r.l. and 2.0 r.l. is reduced slightly by plotting the penetration probability as a function of tray separation in units of gm/cm^2 as shown in Figure 18. Such a plot considers ionization energy losses as opposed to radiation energy losses (units of radiation lengths). There are no scintillation plastic slabs between trays 5 and 6 or 7 and 8 or 9 and 10 as opposed to the other tray combinations. The penetration probability data corresponding to tray combinations 5-6 and 7-8 plotted at 1.4 r.l. are plotted at a smaller depth in a graph of penetration probability as a function of tray separation in units of gm/cm^2. The penetration probabilities associated with tray combinations 5-6 and 7-8 are generally larger than the other tray combinations having the same separation in units of radiation lengths independent of shower energy.

The dispersion in the penetration probability at a given tray separation in units of radiation lengths is due mainly to statistical uncertainties in the covariance in Geiger tube discharges.

The penetration probability is small beyond about 1 r.l. indicating the probability of an electron interacting over a range of about 1 r.l. is large.

2. Proton and sea level cosmic ray meson events. The formalism leading to (V - 27) may be modified to apply to proton and sea level cosmic ray meson events. The selection criteria for these events were the same

as those defining dirty proton events in Chapter III. This selection allows one to analyze events containing interactions defined by multiple tube discharges in a tray. Table XII gives the average number and standard deviation of tube discharges for trays 5 through 10 for these events.

A computer program was used to calculate the covariance in tube discharges for the fifteen tray combinations and the corresponding average number of tube discharges per tray. There were 3567 observed proton events at 2GV and 4765 at 4GVof which, respectively, 501 and 970 satisfied the selection criteria mentioned above. This division of the data resulted in approximately ±15% error in the covariances.

The Geiger tube discharge data for the dirty proton events showed that on the average about 1.5 tubes were discharged per tray while the lateral spread of the proton events in a given tray was around 5 tubes. Hence, the number of tube discharges was approximently equal to the number of particles incident on the trays and capable of discharging Geiger tubes. The covariance of the number of tubes discharged was then assumed to be equal to the covariance of the number of dirty proton event particles. The covariance of the number of dirty proton event Geiger tube discharges was plotted as a function of tray separation. This curve was similar to the covariance curves for electron shower particles.

The average number of particles associated with the dirty proton events was then determined using the method described for electrons. The number was 9.0±1.0 particles and was employed to obtain the penetration probabilities, $\langle N_C \rangle / \langle N_B \rangle$, for the different tray combinations

$$\frac{\langle N_C \rangle}{\langle N_B \rangle} = \frac{\langle n_A \rangle}{N} + \frac{C(n_A, n_B)}{\langle n_B \rangle} \qquad (V - 29)$$

A graph of the proton penetration probability defined by (V - 29) is also given in Figure 17. The proton curve is somewhat higher than that of the electron penetration probability and does not decrease as rapidly at smaller depths. The proton penetration probability approaches zero at large depths.

A similar calculation was carried out for sea level cosmic ray meson events. The Geiger tube discharge information showed that the lateral spread of the events in a given tray was about 4 tubes while there was approximately 1.5 tube discharges per tray. Hence, the average number of tube discharges per tray was assumed equal to the average number of particles incident and capable of discharging a Geiger tube. The resulting values of the penetration probability, defined by (V - 29) and plotted as a function of depth, however, did not fall along a smooth curve as did the electron and proton data. This effect may be partially due to statistical uncertainties since there were only 97 events satisfying the selection criteria, mentioned earlier, out of 2243 observed events.

3. Mean range of electrons, protons, and sea level cosmic ray mesons. The mean range was calculated for the electron showers studied using (V - 4). The results are listed in Table XIII and ranged from 1.04±0.27 r.l. at 1200 MeV to 1.28±0.26 r.l. at 105 MeV. If the dirty proton events mentioned in the previous section are treated as electron-

like showers, then a mean range can be calculated for them using (V - 4). Shower curves were plotted for the dirty proton events and the track lengths were obtained using the method described in Chapter IV. In general, the proton curves were wider than the 1200 MeV electron curve and the shower maxima occurred at more penetrating depths. Combining these track length data with that of Table VIII and (V - 4) results in the proton mean ranges listed in Table XIII. These ranges were about 1.5±0.2 r.l. for the 2 GV and for the 4 GV dirty proton events.

A similar shower curve was plotted for sea level cosmic ray mesons assumed to be electron-like events. The corresponding mean range is given in Table XIII for a maximum depth of 9.3 r.l. The meson shower curve was flat with a magnitude of 1.35 tube discharges/tray. The mean range was 1.5±0.7 r.l. The closeness of the meson range to that of electrons may be due to electron contamination of the data. The meson data was collected on the third floor of a four story building with concrete ceilings. It is possible that meson decays occurred producing electrons $\pi \rightarrow \mu \rightarrow e$.

The mean range of the shower electrons may also be obtained by comparing the experimental penetration probability curves defined by (V -28) with those given by (V - 24) based on a model of electron shower curve slope. Theoretical curves, using (V - 24), were calculated for various values of β, defined by (V - 21), and mean range, R. The electron curve of penetration probability, (V - 28), as a function of tray separation in units of radiation lengths was compared to these theoretical curves to obtain the mean range. The resulting electron mean range for the energy interval studied was 0.9±0.4 r.l. which is consistent with

the values listed in Table XIII for electron mean range based on shower track length and (V - 4).

A similar method was followed for the dirty proton events treated-like-electron-showers. The proton mean range was about 1.7±0.2 r.l. at 2 GV and 1.8±0.2 r.l. at 4 GV which is consistent with the previous calculation using particle track length and (V - 4).

It would appear that the dirty proton events treated -like-electron-showers contain particles that are more effective in discharging Geiger tubes than the particles of electron showers. There are less particles involved in the dirty proton events than in the electron showers although the dirty proton events at 2 GV and 4 GV produce track lengths comparable to a 300 MeV electron shower.

CHAPTER VI

CONCLUSIONS

Three major points have been covered in this study: the response of Geiger tubes to electron showers, fluctuations in electron showers, and correlations in electron showers.

The saturation effect of Geiger tubes for high energy electrons was investigated. A relationship between the average number of particles, $\langle N_A \rangle$, incident and capable of discharging Geiger tubes in tray A (one of trays 5 through 10) and the average number of tubes discharged in tray A, $\langle n_A \rangle_{\langle N_A \rangle}$ was derived,

$$\langle N_A \rangle \simeq \langle n_A \rangle_{\langle N_A \rangle} \left(1 + \alpha \langle n_A \rangle_{\langle N_A \rangle}\right) \qquad \text{(VI - 1)}$$

The saturation effect constant, α, was determined by comparing the average total number of tube discharges in trays 5 through 10 and the average calorimeter pulse height,

$$\alpha = 0.087 \pm 0.009 \qquad \text{(VI - 2)}$$

The constant $\alpha \ll 1$, so the probability of having more than one shower particle incident on a given tube in one of trays 5 through 10 is small. To a first order approximation, the average number of particles incident on and capable of discharging Geiger tubes of a given tray is equal to

the number of tube discharges in that tray.

The electron shower curves computed using (VI-1) and (VI-2) were decidedly different from those found in the literature for other types of detectors. This effect might be the result of the Geiger tubes measuring a different component of electron showers than these other detectors.

The scintillation counter and Geiger tube data were used to calculate electron shower track lengths. A comprehensive comparison of the track length calculations and those from various other experimental and theoretical (Monte Carlo calculations) methods was carried out. The observed track lengths based on scintillation counter pulse heights were in agreement with related measurements in the literature. However, the observed track lengths based on Geiger tube information were perceptibly different from other experimentally determined track lengths.

The resulting track length constants, ε_S and ε_G, based on scintillation counter pulse heights and based on Geiger tube information for electron showers extrapolated to infinite depths were, respectively,

$$\varepsilon_S = 17.2 \pm 1.4 \text{ MeV/r.}\ell. \qquad \text{(VI - 3)}$$

and

$$\varepsilon_G = 34.1 \pm 1.8 \text{ MeV/r.}\ell. \qquad \text{(VI - 4)}$$

In general, the track length constant increases as the shower energy increases for both the Geiger tube and scintillation counter data implying

the rate of energy dissipation is not independent of shower energy. This dependence has been noted in related data in the literature obtained with other types of detectors.

Experimental and theoretical values of track length, track length constant, and shower curve slope past shower maximum are compiled in Table VII.

Track length fluctuations based on scintillation counter pulse heights and Geiger tube information were investigated. A model was devised to relate the shower track length percent fluctuation, σ_T/T, due to the observed percent fluctuation and the intrinsic photoelectron counter percent fluctuation,

$$\frac{\sigma_T}{T} = 28.8\ [(\Delta C_{os})^2 - (\tfrac{4}{3})C_o - C_s(\Delta C_o)^2]^{1/2} \qquad \text{(VI - 5)}$$

The percent fluctuations, σ_T/T, in the track length based on scintillation counter pulse heights was expressed as a power law of the incident electron energy, E_o, in the energy interval $150\text{MeV} < E_o < 1200\text{MeV}$,

$$\frac{\sigma_T}{T} = (36\pm2)\left[\frac{E_o(\text{MeV})}{150\text{MeV}}\right]^{-(0.12\pm0.03)} \qquad \text{(VI - 6)}$$

as shown in Figure 8. Below 150 MeV, the percent fluctuations dropped off sharply.

The percent fluctuations in the track length was also studied using Geiger tube information,

$$\frac{\sigma_T}{T} = 100 \frac{\sigma_{n_{tot}}}{\langle n_{tot} \rangle} \qquad \text{(VI - 7)}$$

A plot of the track length percent fluctuations given by (VI - 7) as a function of incident electron energy, E_o, is shown in Figure 8. These percent fluctuations gradually increased more rapidly as the energy decreased. A model was devised to explain this behavior in terms of percent fluctuation due to sampling uncertainties, $\sigma_T/T\big|_S$,

$$\frac{\sigma_T}{T}\bigg|_S = 100 \left[\frac{1}{\langle n_{tot} \rangle} - \frac{1}{\langle N_{tot} \rangle} \right]^{1/2} \qquad \text{(VI - 8)}$$

and percent fluctuations in the total number of shower particles capable of discharging Geiger tubes, σ_T/T,

$$\frac{\sigma_T}{T} = 100 \left[\frac{1}{\langle n_{tot} \rangle} - \frac{1-Q}{\langle N_{tot} \rangle} \right]^{1/2} \qquad \text{(VI - 9)}$$

where it was assumed $\text{Var } N_{tot} = Q\langle N_{tot} \rangle$ with $0 < Q \leq 1$. The percent fluctuations in the track length based on Geiger tube data given by (VI - 7) was fitted using a combination of (VI - 8) and (VI - 9) with $Q = 0.6$ implying the percent fluctuations in the total number of particles was 74% Poisson.

At lower energies ($105\text{MeV} < E_o < 150\text{MeV}$), the percent fluctuations in track length based on scintillation counter pulse heights and based on Geiger tube data shown in Figure 8 have vastly different dependences

on incident electron energy. However, the curves approximating the two sets of data appear to approach a constant negative slope of about -0.12 for energies $E_o > 300$ MeV.

The dependence of the variance in Geiger tube discharges was studied. The tube variances were compared, as a function of electron shower depth, at a standard energy of 1000 MeV with theoretical curves (Monte Carlo calculations) and data from other types of detectors. These detectors included a lucite Cerenkov counter, scintillation counters, and a multiplate cloud chamber. The variance in tube discharges was found to be noticeably less steep past variance maximum.

The correlation in Geiger tube discharges for the fifteen combinations of trays was investigated for electron showers, proton events, and sea level cosmic ray meson events. The covariances of Geiger tube discharges for these particles are positive at small tray separations but decrease rapidly as a function of tray separation and approach constant negative values. The observed dispersion in experimental covariances at a given depth was found not to be energy dependent for electron showers and probably is due to statistical uncertainties in the data.

A model was devised to relate the covariance in number of particles incident on the Geiger tube trays to the average number of particles passing through the trays and the average total number of shower particles, N,

$$C(N_A,N_B) = \langle N_C \rangle - \frac{\langle N_A \rangle \langle N_B \rangle}{N} \qquad (VI - 10)$$

This covariance was in turn related to the covariance in the corresponding number of Geiger tubes discharged,

$$C(N_A,N_B) = [\ 1 + 2\alpha(\langle n_A \rangle + \langle n_B \rangle)\ ]\ C(n_A,n_B) \qquad (VI - 11)$$

The covariance contribution due to penetrating particles is represented by, $\langle N_C \rangle$, in (VI-10) and the contribution due to particles passing through tray A and due to particles passing through tray B is denoted by, $-\langle N_A \rangle \langle N_B \rangle$, in (VI-10). The average total number of shower particles, N, was then obtained using (VI-10), (VI-11) and ranged from 4.0±0.7 at 105 MeV to 36.6±6.5 at 1200 MeV. A plot of the average number of shower particles as a function of incident electron energy is given in Figure 15. The number of shower particles rises slowly in the energy region from 105 MeV to 300 MeV and then increases linearly with the incident electron energy. The total number of shower particles is related to the shower energy in the energy interval 105 MeV<E<1200MeV by

$$N = (0.029 \pm 0.003)E(MeV) \qquad (VI - 12)$$

A modified form of (VI-10) and (VI-11) is used to obtain the average total number of particles associated with the proton events and sea level

cosmic ray meson events. The resulting numbers were 1.8±0.2 particles for 2 GV and 4 GV proton events and 1.5±0.7 particles for the sea level cosmic ray meson events.

The electron showers were also analyzed using the concept of penetration probability, $\langle N_C \rangle / \langle N_B \rangle$, defined as the probability that a particle present at depth, x, has penetrated from a depth, x - t,

$$\frac{\langle N_C \rangle}{\langle N_B \rangle} = \frac{\langle n_A \rangle (1 + \alpha \langle n_A \rangle)}{N} + \frac{C(n_A, n_B) \; [\; 1 + 2\alpha (\langle n_A \rangle + \langle n_B \rangle) \;]}{\langle n_B \rangle (1 + \alpha \langle n_B \rangle)} \qquad \text{(VI - 13)}$$

The resulting penetration probabilities are plotted as a function of tray separation in Figure 17. These data are a sharply decreasing function of tray separation for depths less than 1 r.l. and approach zero more gradually at larger depths. The dispersion in the electron penetration probability at a given depth was found not to be dependent on shower energy. It was also found not to depend on the mean depth of the Geiger tube trays associated with the covariance term in the penetration probability equation (VI-13). The dispersion in the probability at a given depth is more likely due to the statistical uncertainties in the covariance of Geiger tube discharges.

A modified form of (VI-13) was applied to the proton event data. The resulting penetration probabilities are plotted as a function of tray separation in Figure 17 assuming the proton events are made up of electron-like-particles. The proton curve is somewhat above the electron penetration probability curve and does not decrease as rapidly at small depths. A similar calculation was carried out for sea level cosmic ray

meson events, however, the resulting values of penetration probability did not fall along a smooth curve as a function of tray separation. This result may be partially due to statistical uncertainties since there were only 97 events satisfying the selection criteria used out of 2243 observed events.

The Geiger tube discharge probability distribution was investigated for trays 5 through 10 for electron showers, proton events, and sea level cosmic ray meson events. The resulting experimental probabilities are listed in Tables IX, X, and XI, respectively. Binomial probability distributions were calculated for these trays using the average number of tubes discharged and the average total number of particles in the shower derived from (VI-10)and (VI-11) This method neglects the second order saturation effect. A Poisson probability distribution was also calculated for each experimental distribution.

The two theoretical distributions approximate the experimental distribution points equally well over a range of probabilities from 0.001 to 1.0. A similar procedure was followed for the proton and sea level cosmic ray meson Geiger tube discharge data. It was found that the proton and meson events induced about the same tube discharge distributions and could not be distinguished from those caused by electron showers.

The mean range, R, of electron shower particles, proton event particles, and sea level cosmic ray meson event particles was calculated using track length data based on Geiger tube information,

$$R = T/N \qquad \text{(VI - 14)}$$

and using the penetration probability curves. It was found that the two methods gave consistent results of about 1.0±0.4 r.l. for electron shower particles in the energy interval 105MeV<E<1200 MeV, 1.8±0.2 r.l. for 1300 MeV and 3200 MeV proton event particles, and 1.5±0.7 r.l. for sea level cosmic ray meson event particles. The meson range is questionable due to poor statistics and possible contamination of the data by electrons.

The derived information from this investigation is useful in design of detectors and might lead to a method of separating electrons from protons and other particles in a cosmic ray beam.

REFERENCES

REFERENCES

Backenstoss, G., Hyams, B.D., Knop, G., and Stierlin, U. 1963, Nucl. Instr. Methods, 21, 155.

Becklin, E.E., and Earl, J.A. 1964, Phys. Rev., 136, B237.

Belen 'kii, S.Z., and Ivanenko, I.P. 1960, Soviet Phys. - Usp. 2, 912.

Beuermann, K., and Wibberenz, G. 1967, Z. Physik, 206, 247.

Blocker, W., Kenney, R.W., and Panofsky, W.K. 1950, Phys. Rev., 79, 419.

Butcher, J.C., and Messel, H. 1960, Nuclear Phys., 20, 15.

Crannell, C.J. 1967, Phys. Rev., 161, 310.

Crawford, D.F., and Messel, H. 1962, Phys. Rev., 128, 2352.

Cronin, J.W., Engels, E., Pyka, M., and Roth, R. 1962, Rev. Sci. Inst., 33, 946.

Drickey, D.J., Kilner, J.R., and Benaksas, D. 1968, Phys. Rev., 171, 310.

Fitch, V.L., Meyer, S.L., and Piroué, P.A. 1962, Phys. Rev., 126, 1849.

Heusch, C.A., and Prescott, C.Y. 1964, Phys. Rev., 135, B772.

Jenkins, T.M., Cobb, J.K., Nelson, W.R., and McCall, R.C. 1965, Nucl. Instr. Methods, 37, 174.

Kajikawa, R. 1963, J. Phys. Soc. Japan, 18, 1365.

Kantz, A., and Hofstadter, R. 1953, Phys. Rev., 89, 607.

Kantz, A., and Hofstadter, R. 1954, Nucleonics, 12, 36.

Lengeler, H., Deutschmann, M., and Tejessy, W. 1963, Nuovo Cimento, 28, 1501.

Messel, H., Smirnov, A.D., Varfolomeev A.A., Crawford, D.F. and Butcher, J.L. 1962, Nuclear Phys., 39, 1.

Murata, Y. 1965, J. Phys. Soc. Japan, 20, 209.

Nagel, H. 1965, Z. Physik, 186, 319.

Neely, D.E. 1968,Master's Thesis, University of Maryland Department of Physics and Astronomy Technical Report No. 845.

Nelson, W.R., Jenkins, T.M., Mc Call, R.C., and Cobb, J.K. 1966, Phys. Rev., 149, 201.

Rossi, B. 1952, High Energy Particles (Englewood, New Jersey: Prentice-Hall, Inc.).

Rossi, B., and Greisen, K. 1941, Revs. Modern Phys., 13, 240.

Snyder, H. 1938, Phys. Rev., 53, 960.

Thom, H. 1964, Phys. Rev., 136, B447.

Wilson, R.R. 1952, Phys. Rev. 86, 261.

APPENDIX

TABLES AND FIGURES

TABLE I

PULSE HEIGHT ANALYZER CHANNEL FACTORS

	PHA CHANNEL FACTORS†									
	.0	.1	.2	.3	.4	.5	.6	.7	.8	.9
0	1.00	1.029	1.059	1.088	1.124	1.155	1.188	1.223	1.259	1.296
1	1.33	1.37	1.41	1.45	1.50	1.54	1.58	1.63	1.68	1.73
2	1.78	1.83	1.88	1.94	1.99	2.05	2.11	2.17	2.24	2.30
3	2.37	2.44	2.51	2.54	2.66	2.74	2.82	2.90	2.98	3.07
4	3.16	3.25	3.34	3.44	3.54	3.64	3.75	3.86	3.97	4.09
5	4.21	4.33	4.46	4.59	4.72	4.86	5.00	5.14	5.30	5.45
6	5.61	5.77	5.95	6.11	6.30	6.48	6.68	6.87	7.07	7.28
7	7.49	7.70	7.92	8.15	8.40	8.63	8.90	9.14	9.41	9.70
8	10.0									

†Read for example; 3.2 channels = factor of 2.51 in pulse height.

TABLE II

SUMMARY OF EVENTS ANALYZED

Rigidity (MV)	Comments	No. of Tubes Discharged	No. Events Observed	No. Events Acceptable	% Events Accepted
2000	Proton events	36 630	3567	3100	87
4000	Proton events	53 323	4765	4230	89
	Sea level cosmic ray meson events	25 171	2243	1789*	80
105	Electron showers	19 145	2829	2439	86
150	Electron showers	25 892	3442	3049	89
300	Electron showers	36 859	3594	3136	87
600	Electron showers	49 404	3607	3132	87
1000	Electron showers with detector inclined 10^{o} to incident beam	62 812	3721	3169	85
1200	Electron showers	93 430	5117	4452	87

* The acceptance criterion was that there be no multiple tube discharges per tray in trays 1 through 10.

TABLE III

SCINTILLATION COUNTER PULSE HEIGHTS

Rigidity (MV)	Comments	$\left\langle \frac{dE}{dx} \right\rangle$ † (channels)	$\sigma_{dE/dx}$ (channels)	<Cal> † (channels)	σ_{Cal} (channels)
2000& 4000	Dirty proton events*	5.49±0.04	1.35±0.04	7.17±0.08	2.81±0.05
2000& 4000	Clean proton events*	5.34±0.17	1.23±0.02	3.03±0.03	1.69±0.02
2000& 4000	Dirty proton events**	5.50±0.05	1.31±0.05	7.26±0.11	3.04±0.07
2000& 4000	Clean proton events**	5.34±0.03	1.27±0.02	3.05±0.03	1.67±0.03
	Sea level cosmic ray meson events††	3.61±0.09	1.52±0.23	3.16±0.08	1.58±0.24
105	Electron shower	5.29±0.03	1.27±0.03	2.49±0.05	2.01±0.03
150	Electron shower	5.36±0.03	1.35±0.03	3.33±0.04	2.03±0.02
300	Electron shower	5.38±0.03	1.28±0.02	5.49±0.03	1.63±0.03
600	Electron shower	5.54±0.02	1.30±0.02	7.53±0.03	1.37±0.02
1200	Electron shower	5.73±0.02	1.33±0.02	9.36±0.02	1.16±0.02

† $\left\langle \frac{dE}{dx} \right\rangle$ and $\langle Cal \rangle$ represent, respectively, the average pulse height for the dE/dx and calorimeter counters.

†† The selection criteria for these events was that there be one and only one tube discharge per tray in the first four Geiger tube trays of the detector.

* These data are for experimental runs with the lead shield in front of the detector.

** These data are for experimental runs with no lead shield in front of the detector.

TABLE IV

PERCENT FLUCTUATION IN TRACK LENGTH BASED

ON SCINTILLATION COUNTER PULSE HEIGHTS

Energy (MeV)	$\Delta P_i/P_i$ (%)	$\Delta P_s/P_s$ (%)
105	51.9±0.9	25.7±1.0
150	46.3±0.8	35.8±1.4
300	33.8±0.6	32.5±1.4
600	25.1±0.5	30.5±0.9
1200	19.4±0.3	27.2±0.8

TABLE V

AVERAGE NUMBER AND VARIANCE OF GEIGER TUBE DISCHARGES OF ELECTRON SHOWERS

Tray No.	Depth* (r.ℓ.)	105 MeV		150 MeV		300 MeV		600 MeV		1000 MeV		1200 MeV	
		$\langle n \rangle$**	σ^{2}**	$\langle n \rangle$	σ^2	$\langle n \rangle$	σ^2	$\langle n \rangle$	σ^2	$\langle n \rangle$	σ^2	$\langle n \rangle$	σ^2
5	1.57	1.12	0.78	1.25	0.79	1.52	0.87	1.69	1.02	1.84	1.18	1.85	1.03
6	2.95	0.70	0.77	0.93	0.92	1.50	1.14	1.88	1.30	2.15	1.55	2.29	1.56
7	4.37	0.37	0.48	0.56	0.72	1.25	1.20	2.09	1.52	2.67	1.95	2.90	1.83
8	5.76	0.25	0.33	0.35	0.44	0.90	0.99	1.72	1.35	2.35	1.76	2.69	1.85
9	7.18	0.13	0.18	0.21	0.27	0.61	0.80	1.33	1.38	2.17	1.87	2.49	1.84
10	9.22	0.08	0.11	0.11	0.15	0.35	0.54	0.85	1.08	1.47	1.57	1.88	1.80

* Only one particle should pass through tray 4 at a time.

** $\langle n \rangle$ and σ^2 are in units of Geiger tubes discharged.

TABLE VI

PERCENT FLUCTUATIONS IN TRACK LENGTH BASED

ON GEIGER TUBE DISCHARGES

Energy (MeV)	σ_T/T (%)	$\langle n_{tot} \rangle$*	$\sigma_{n_{tot}}$*
105	59.5±1.8	2.57±0.06	1.53±0.03
150	49.6±1.5	3.42±0.08	1.70±0.03
300	32.7±0.8	6.42±0.13	2.11±0.03
600	26.1±0.6	9.82±0.18	2.56±0.04
1200	22.3±0.4	14.23±0.22	3.17±0.04

* The quantities $\langle n_{tot} \rangle$ and $\langle \sigma_{n_{tot}} \rangle$ are expressed in units of Geiger tubes discharged.

TABLE VII

SUMMARY OF ELECTRON SHOWER PARAMETERS

Source	Energy (MeV)	Depth (r.ℓ.)	Track Length (r.ℓ.)	Slope^{-1} (r.ℓ.)$^{-1}$	ε (MeV/r.ℓ.)
Observed- Geiger tube	105	9.31	4.9±0.5		
		∞	5.1±0.5	0.40±0.05	20.8±3.7
	150	9.31	6.1±0.6		
		∞	6.4±0.6	0.40±0.05	23.4±4.0
	300	9.31	10.5±1.1		
		∞	11.7±1.1	0.32±0.05	25.7±4.6
	600	9.31	16.4±1.7		
		∞	20.1±2.1	0.25±0.08	29.9±5.5
	1000	9.31	21.9±2.3		
		∞	30.1±4.1	0.20±0.08	33.2±6.7
	1200	9.31	24.5±2.5		
		∞	37.8±7.1	0.16±0.08	31.8±7.6
Observed - Scintillation Counter	105	7.2	6.79±0.30		
		∞	7.30±0.30	...	14.38±0.59
	150	7.2	8.44±0.30		
		∞	9.62±0.31	...	15.59±0.50
	300	7.2	14.93±0.60		
		∞	18.90±0.66	...	15.87±0.55
	600	7.2	26.60±1.00		
		∞	36.94±1.23	...	16.24±0.54
	1200	7.2	44.55±1.70		
		∞	62.29±2.05	...	19.26±0.63
Becklin and Earl, 1964	500	7	16.1±1.5		
		∞	20.2±2.0	0.31±0.06	24.8±2.5

TABLE VII (continued)

Source	Energy (MeV)	Depth (r.ℓ.)	Track Length (r.ℓ.)	Slope^{-1} (r.ℓ.)$^{-1}$	ε (MeV/r.ℓ.)
Becklin and Earl, 1964	1000	7	31.1±1.5		
		∞	43.7±3.0	0.26±0.06	23.0±2.0
	500–1000	∞	...	...	23.6±1.6
Thom, 1964	277	9.5	11.8		
		∞	13.0	...	21.5**
	528	9.5	20.3		
		∞	22.5	...	21.9**
	845	9.5	30.7		
		∞	37.0	...	23.5**
	990	9.5	34.4		
		∞	41.0	...	23.7**
Neely, 1968	105	9	6.5±0.4		
		∞	6.9±0.5	0.39±0.03	15.3±1.0
	150	9	9.3±0.6		
		∞	10.0±0.6	0.34±0.02	15.1±1.0
	300	15	19.1±1.2		
		∞	19.5±1.2	0.29±0.02	15.4±1.0
	600	18	35.7±2.2		
		∞	36.3±2.2	0.29±0.02	16.6±1.0
	1000	18	57.4±3.5		
		∞	58.5±3.6	0.30±0.02	17.1±1.1
	1200	18	65.8±4.1		
		∞	67.2±4.1	0.31±0.02	17.9±1.1

TABLE VII (continued)

Source	Energy (MeV)	Depth (r.ℓ.)	Track Length (r.ℓ.)	Slope^{-1} (r.ℓ.)	ε (MeV/r.ℓ.)
Beuermann and Wibberenz, 1967	200,400	10	...	0.264	22
Backenstoss, Hyams, Knop, and Stierlin, 1963	3000	∞	314*	0.41*	9.6*
Heusch and Prescott, 1964	500	10	15.6*	...	...
	1000	10	31.4*	...	...
	100–1000	∞	...	0.26	28.6
Drickey, Kilner, and Benaksas, 1968	1000	10	20.0*	0.14*	50*
Kajikawa, 1963	550	10	15.7*	...	35.03*
Cronin, Engels, Pyka, and Roth, 1962	193	10	8.9*	...	21.7*
	600	10	12.7*	...	47.2*
Lengeler, Deutschmann and Tejessy, 1963	92–372	∞	...	0.25*	21.1±1.3

TABLE VII (continued)

Source	Energy (MeV)	Depth (r.ℓ.)	Track Length (r.ℓ.)	Slope^{-1} (r.ℓ.)	ε (MeV/r.ℓ.)
Crawford and Messel, 1962 (Monte Carlo calculation with E_{co}=10 MeV)	100	9	3.18	0.26*	31.45
	500	9	14.9	0.17*	33.56*
	1000	9	28.6	0.12*	34.97*
	50–1000	∞	...	...	31.25

* This datum was computed, here, from data given in the reference.

** Thom found that the track length, T, and incident electron energy, E, are related by

$$T = 0.073E^{0.92}$$

based on observations of 300 showers.

TABLE VIII

AVERAGE NUMBER OF SHOWER PARTICLES BASED ON GEIGER TUBE DISCHARGES

Comment	Energy (MeV)	No. of particles
Electron shower	105	4.0 ± 0.7
	150	5.0 ± 1.0
	300	7.5 ± 1.3
	600	15.5 ± 3.0
	1000	28.0 ± 5.0
	1200	36.5 ± 6.5
Dirty proton event	1300	9.0 ± 1.0
	3200	10.5 ± 1.5
Sea level cosmic ray meson event*	-	8.0 ± 3.6

* These events satisfied the same selection criteria as that of dirty proton events.

TABLE IX

GEIGER TUBE DISCHARGE PROBABILITY DISTRIBUTIONS FOR ELECTRON SHOWERS

Energy (MeV)	No. tubes discharges	Probability tray 5	tray 6	tray 7	tray 8	tray 9	tray 10
105	0	.2124±.0093	.5051±.0144	.7204±.0172	.8052±.0182	.8930±.0191	.9405±.0196
	1	.5506±.0150	.3448±.0119	.2099±.0093	.1525±.0079	.0877±.0060	.0447±.0043
	2	.1706±.0084	.1111±.0067	.0537±.0047	.0320±.0036	.0144±.0024	.0115±.0022
	3	.0488±.0045	.0287±.0034	.0111±.0021	.0082±.0018	.0041±.0013	.0038±.0012
	4	.0119±.0022	.0057±.0015	.0037±.0012	.0021±.0009	.0004±.0004	0
	5	.0041±.0013	.0037±.0012	.0008±.0006	0	.0004±.0004	0
	6	.0012±.0007	.0008±.0006	.0004±.0004	0	0	0
	7	.0004±.0004	0	0	0	0	0
	8	0	0	0	0	0	0
	9	0	0	0	0	0	0

TABLE IX (continued)

Energy (MeV)	No. tubes discharges	Probability tray 5	tray 6	tray 7	tray 8	tray 9	tray 10
150	0	.1525±.0071	.3772±.0111	.6100±.0141	.7370±.0155	.8363±.0166	.9082±.0173
	1	.5526±.0135	.3985±.0114	.2676±.0094	.1955±.0080	.1279±.0065	.0751±.0050
	2	.2109±.0083	.1614±.0073	.0902±.0054	.0538±.0042	.0285±.0031	.0134±.0021
	3	.0607±.0045	.0430±.0038	.0216±.0027	.0102±.0018	.0066±.0015	.0020±.0008
	4	.0194±.0025	.0164±.0023	.0069±.0015	.0033±.0010	.0003±.0003	.0013±.0007
	5	.0033±.0010	.0030±.0010	.0030±.0010	.0003±.0003	.0003±.0003	0
	6	0	.0007±.0005	.0003±.0003	0	0	0
	7	.0007±.0005	0	.0003±.0003	0	0	0
	8	0	0	0	0	0	0
	9	0	0	0	0	0	0

TABLE IX (continued)

Energy (MeV)	No. tubes discharges	Probability tray 5	tray 6	tray 7	tray 8	tray 9	tray 10
300	0	.0759±.0049	.1327±.0065	.2749±.0094	.4196±.0116	.5858±.0137	.7510±.0155
	1	.5045±.0127	.4506±.0120	.3699±.0109	.3527±.0106	.2736±.0093	.1757±.0075
	2	.2937±.0097	.2761±.0093	.2357±.0087	.1620±.0072	.0979±.0056	.0526±.0041
	3	.0934±.0055	.0938±.0055	.0839±.0052	.0472±.0039	.0313±.0032	.0143±.0021
	4	.0230±.0027	.0313±.0032	.0261±.0029	.0128±.0020	.0073±.0015	.0032±.0010
	5	.0064±.0014	.0108±.0019	.0070±.0015	.0032±.0010	.0038±.0011	.0022±.0008
	6	.0032±.0010	.0029±.0010	.0019±.0008	.0026±.0009	0	.0006±.0005
	7	0	.0016±.0007	.0006±.0005	0	.0003±.0003	.0003±.0003
	8	0	0	0	0	0	0
	9	0	.0003±.0003	0	0	0	0

TABLE IX (continued)

Energy (MeV)	No. tubes discharges	Probability tray 5	tray 6	tray 7	tray 8	tray 9	tray 10
600	0	.0453±.0038	.0632±.0045	.0808±.0051	.1293±.0064	.2743±.0094	.4751±.0123
	1	.4658±.0122	.3471±.0105	.2337±.0086	.3388±.0104	.3337±.0103	.3043±.0099
	2	.3250±.0102	.3611±.0107	.3669±.0108	.3151±.0100	.2433±.0088	.1440±.0070
	3	.1076±.0059	.1472±.0069	.2075±.0081	.1443±.0068	.1038±.0058	.0530±.0041
	4	.0390±.0035	.0517±.0041	.0738±.0049	.0527±.0041	.0300±.0031	.0179±.0024
	5	.0121±.0020	.0201±.0025	.0255±.0029	.0166±.0023	.0109±.0019	.0038±.0011
	6	.0038±.0011	.0070±.0015	.0077±.0016	.0019±.0008	.0032±.0010	.0019±.0008
	7	.0010±.0006	.0022±.0008	.0032±.0010	.0010±.0006	.0010±.0006	0
	8	.0003±.0003	.0003±.0003	.0010±.0006	.0003±.0003	0	0
	9	0	0	0	0	0	0

TABLE IX (continued)

Energy (MeV)	No. tubes discharges	Probability tray 5	tray 6	tray 7	tray 8	tray 9	tray 10
1000	0	.0379±.0035	.0461±.0038	.0382±.0035	.0615±.0044	.0972±.0055	.2455±.0088
	1	.4039±.0113	.2790±.0094	.1496±.0069	.2020±.0080	.2367±.0086	.3212±.0101
	2	.3537±.0106	.3563±.0106	.3111±.0099	.3225±.0101	.3001±.0097	.2405±.0087
	3	.1297±.0064	.1859±.0077	.2588±.0090	.2430±.0088	.2083±.0081	.1284±.0064
	4	.0476±.0039	.0830±.0051	.1426±.0067	.1098±.0059	.1022±.0057	.0429±.0037
	5	.0196±.0025	.0353±.0033	.0625±.0044	.0407±.0036	.0376±.0034	.0161±.0023
	6	.0050±.0013	.0104±.0018	.0284±.0030	.0161±.0023	.0148±.0022	.0044±.0012
	7	.0016±.0007	.0038±.0011	.0069±.0015	.0032±.0010	.0028±.0009	.0009±.0005
	8	.0009±.0005	.0003±.0003	.0016±.0007	.0013±.0006	.0003±.0003	0
	9	0	0	.0003±.0003	0	0	0

TABLE IX (continued)

Energy (MeV)	No. tubes discharges	Probability tray 5	tray 6	tray 7	tray 8	tray 9	tray 10
1200	0	.0204±.0021	.0236±.0023	.0168±.0019	.0283±.0025	.0512±.0034	.1453±.0057
	1	.4057±.0095	.2576±.0076	.1049±.0049	.1465±.0057	.1830±.0064	.2850±.0080
	2	.3742±.0092	.3551±.0089	.2994±.0082	.3176±.0084	.3062±.0083	.2846±.0080
	3	.1352±.0055	.2138±.0069	.2873±.0080	.2677±.0078	.2502±.0075	.1716±.0062
	4	.0435±.0031	.0943±.0046	.1772±.0063	.1444±.0057	.1354±.0055	.0770±.0042
	5	.0148±.0018	.0350±.0028	.0728±.0040	.0645±.0038	.0514±.0034	.0252±.0024
	6	.0036±.0009	.0159±.0019	.0299±.0026	.0209±.0022	.0166±.0019	.0070±.0013
	7	.0020±.0007	.0038±.0009	.0081±.0013	.0065±.0012	.0047±.0010	.0036±.0009
	8	.0004±.0003	.0002±.0002	.0027±.0008	.0029±.0008	.0007±.0004	.0007±.0004
	9	0	.0004±.0003	.0009±.0004	.0007±.0004	.0004±.0003	0

TABLE X

GEIGER TUBE DISCHARGE PROBABILITY DISTRIBUTIONS FOR DIRTY PROTON EVENTS

Rigidity (MV)	No. tubes discharges	Probability tray 5	tray 6	tray 7	tray 8	tray 9	tray 10
2000	0	.0299±.0077	.0299±.0077	.0998±.0141	.1038±.0144	.1896±.0195	.2754±.0234
	1	.7246±.0380	.6208±.0352	.4691±.0306	.4451±.0298	.4032±.0284	.3733±.0237
	2	.1477±.0172	.1776±.0188	.2315±.0215	.1976±.0199	.1956±.0198	.1577±.0177
	3	.0579±.0107	.1178±.0153	.1238±.0157	.1796±.0189	.1377±.0166	.1078±.0147
	4	.0120±.0063	.0319±.0080	.0419±.0091	.0399±.0089	.0419±.0091	.0399±.0089
	5	.0120±.0049	.0120±.0049	.0260±.0072	.0200±.0063	.0240±.0069	.0240±.0069
	6	.0060±.0035	.0060±.0035	.0040±.0028	.0080±.0040	.0080±.0040	.0180±.0060
	7	.0020±.0020	.0040±.0028	.0020±.0020	.0040±.0028	0	.0020±.0020
	8	0	0	.0020±.0020	.0020±.0020	0	.0020±.0020
	9	0	0	0	0	0	0

TABLE X (continued)

Rigidity (MV)	No. tubes discharges	Probability tray 5	tray 6	tray 7	tray 8	tray 9	tray 10
4000	0	.0165±.0041	.0165±.0041	.0186±.0044	.0381±.0063	.0814±.0092	.1505±.0125
	1	.7309±.0275	.7309±.0275	.6433±.0258	.4124±.0206	.3093±.0179	.2763±.0169
	2	.1206±.0112	.1206±.0112	.1598±.0128	.2454±.0159	.2742±.0168	.2186±.0150
	3	.0742±.0087	.0742±.0087	.0990±.0101	.1639±.0130	.1598±.0128	.1928±.0141
	4	.0340±.0059	.0340±.0060	.0505±.0072	.0763±.0089	.1052±.0104	.0918±.0097
	5	.0113±.0034	.0113±.0034	.0113±.0034	.0423±.0066	.0320±.0057	.0381±.0063
	6	.0062±.0025	.0062±.0025	.0082±.0029	.0144±.0039	.0237±.0049	.0196±.0045
	7	.0041±.0021	.0041±.0021	.0062±.0025	.0041±.0021	.0093±.0031	.0103±.0033
	8	.0021±.0015	.0021±.0015	.0031±.0018	.0021±.0015	.0021±.0015	.0021±.0015
	9	0	0	0	.0010±.0010	.0031±.0018	0

TABLE XI

GEIGER TUBE DISCHARGE PROBABILITY DISTRIBUTIONS

FOR SEA LEVEL COSMIC RAY MESON EVENTS*

No. tubes discharged	Probability tray 5	tray 6	tray 7	tray 8	tray 9	tray 10
0	.7010±.0850	.0412±.0206	.0825±.0292	.0825±.0292	.1340±.0372	.1649±.0412
1	.1443±.0386	.7216±.0863	.6082±.0792	.6186±.0799	.5979±.0785	.5464±.0751
2	.1237±.0357	.1546±.0399	.1959±.0449	.1645±.0412	.1443±.0386	.1546±.0399
3	.0206±.0146	.0619±.0253	.0722±.0273	.1031±.0326	.0928±.0309	.0928±.0309
4	.0103±.0103	0	.0412±.0206	.0309±.0179	.0309±.0179	.0206±.0146
5	0	.0206±.0146	0	0	0	.0103±.0103
6	0	0	0	0	0	0
7	0	0	0	0	0	0
8	0	0	0	0	0	.0103±.0103
9	0	0	0	0	0	0

*These events satisfy the same selection criteria as those for dirty proton events.

TABLE XII

AVERAGE NUMBER AND STANDARD DEVIATION OF

GEIGER TUBE DISCHARGES OF DIRTY PROTON EVENTS AND

SEA LEVEL COSMIC RAY MESON EVENTS

Tray No.	Depth* (r.ℓ.)	2GV† <n>**	2GV† σ**	4GV† <n>	4GV† σ	Mesons†† <n>	Mesons†† σ
5	1.57	1.38	0.93	1.47	1.05	1.50	0.86
6	2.95	1.58	1.06	1.64	1.18	1.32	0.82
7	4.37	1.66	1.21	1.96	1.33	1.38	0.89
8	5.76	1.73	1.27	2.05	1.37	1.38	0.89
9	7.18	1.54	1.27	2.17	1.52	1.29	0.92
10	9.22	1.43	1.43	2.06	1.56	1.35	1.19

* Only one particle should pass through tray 4 at a time.

** <n> and σ are in units of Geiger tubes discharged.

† Dirty proton events.

†† Sea level cosmic ray meson events satisfying the same selection criteria as that for dirty proton events.

TABLE XIII

MEAN RANGE OF SHOWER PARTICLES BASED ON GEIGER TUBE DISCHARGES

Comment	Energy (MeV)	Mean Range Track Length (r.ℓ.)	Penetration Prob.
Electron shower	105	1.28±0.26	
	150	1.28±0.28	
	300	1.56±0.31	0.9±0.4*
	600	1.30±0.29	
	1000	1.08±0.24	
	1200	1.04±0.27	
Proton event	1300	1.56±0.17	1.7±0.2
	3200	1.53±0.22	1.8±0.2
Sea level cosmic ray meson event**	-	1.50±0.68	-

* The mean range obtained using the penetration probability curve applies to the energy range 105 MeV < E_o < 1200 MeV.

** The track length used in this calculation cooresponded to a maximum depth of 9.3 r.ℓ. These events satisfied the same selection criteria as that of dirty proton events.

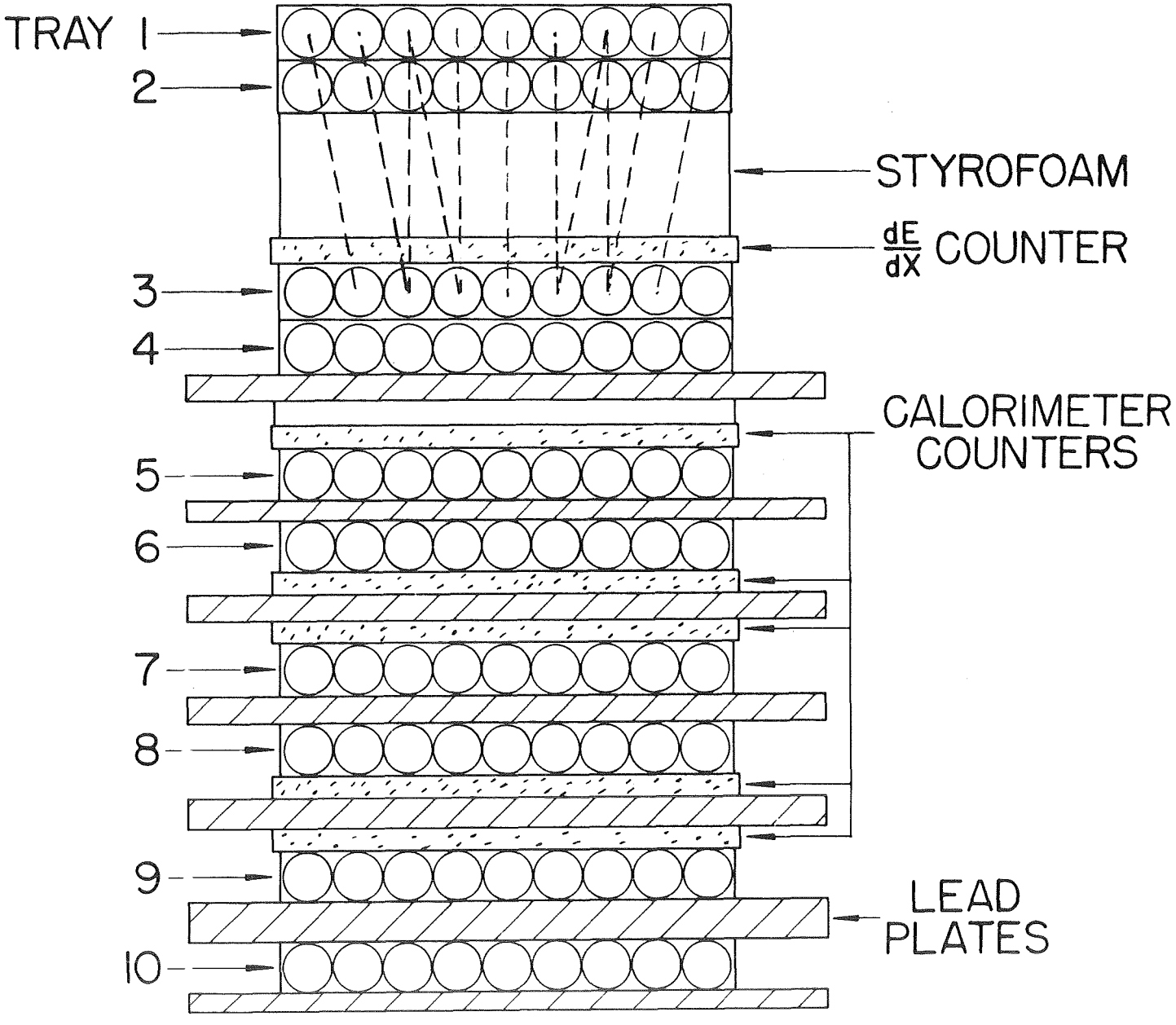
TRAY 1
2
3
4
5
6
7
8
9
10
STYROFOAM
dE/dX COUNTER
CALORIMETER COUNTERS
LEAD PLATES

Fig. 1

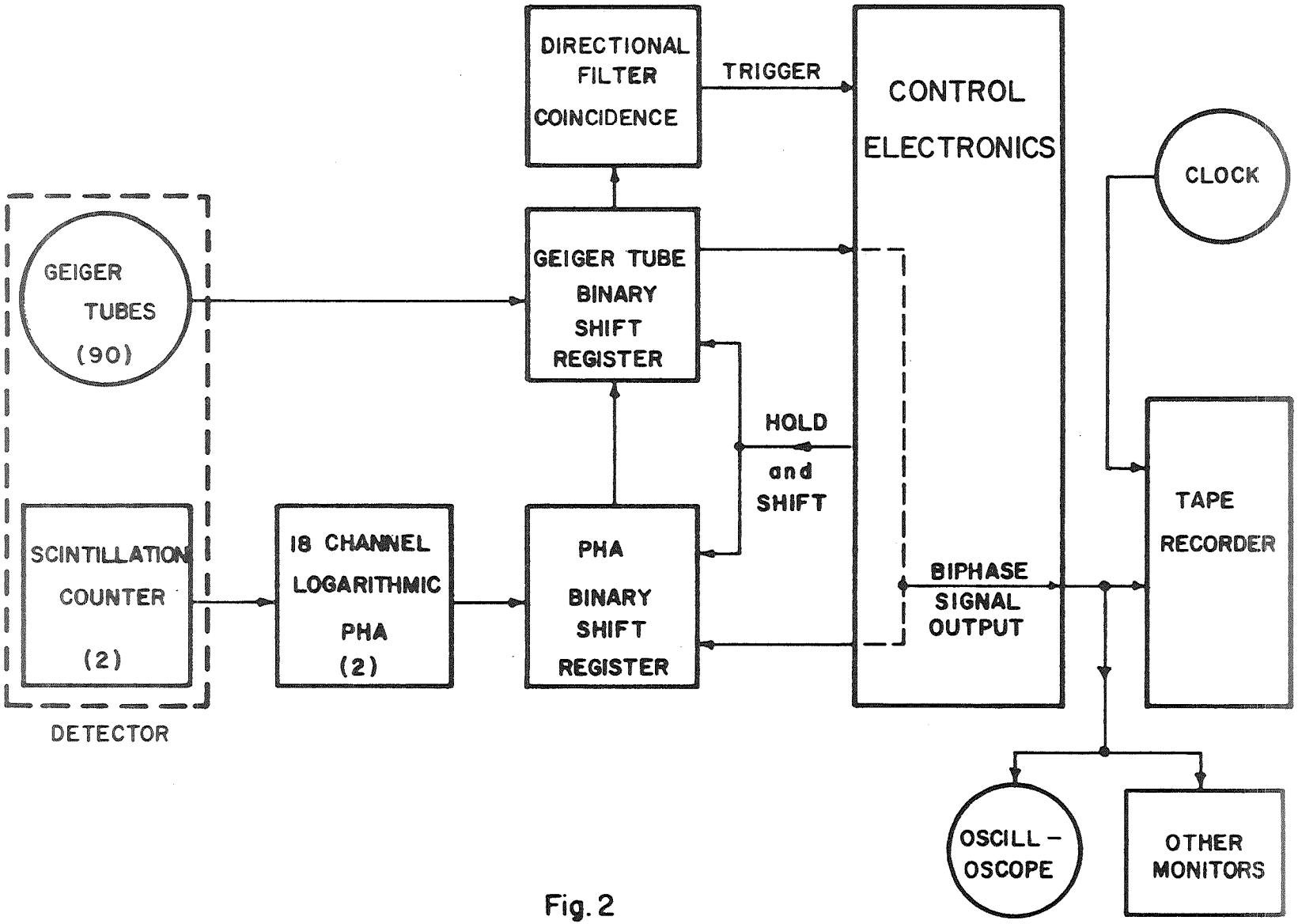
DIRECTIONAL FILTER COINCIDENCE
TRIGGER
CONTROL ELECTRONICS
CLOCK
GEIGER TUBES (90)
GEIGER TUBE BINARY SHIFT REGISTER
HOLD and SHIFT
TAPE RECORDER
SCINTILLATION COUNTER (2)
18 CHANNEL LOGARITHMIC PHA (2)
PHA BINARY SHIFT REGISTER
BIPHASE SIGNAL OUTPUT
DETECTOR
OSCILL-OSCOPE
OTHER MONITORS

Fig. 2

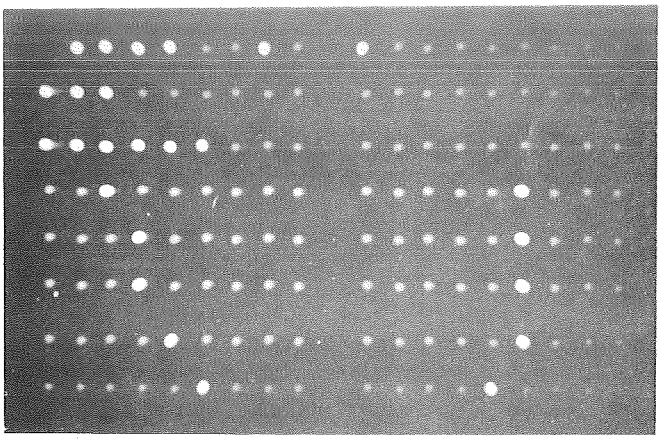

MESON

3a

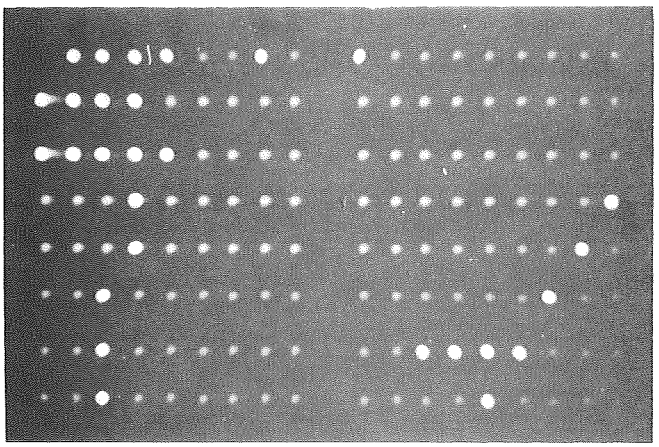

PROTON

3b

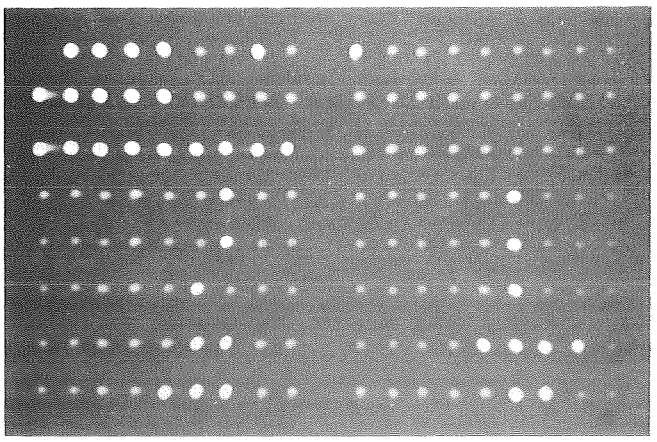

ELECTRON

3c

Fig. 3

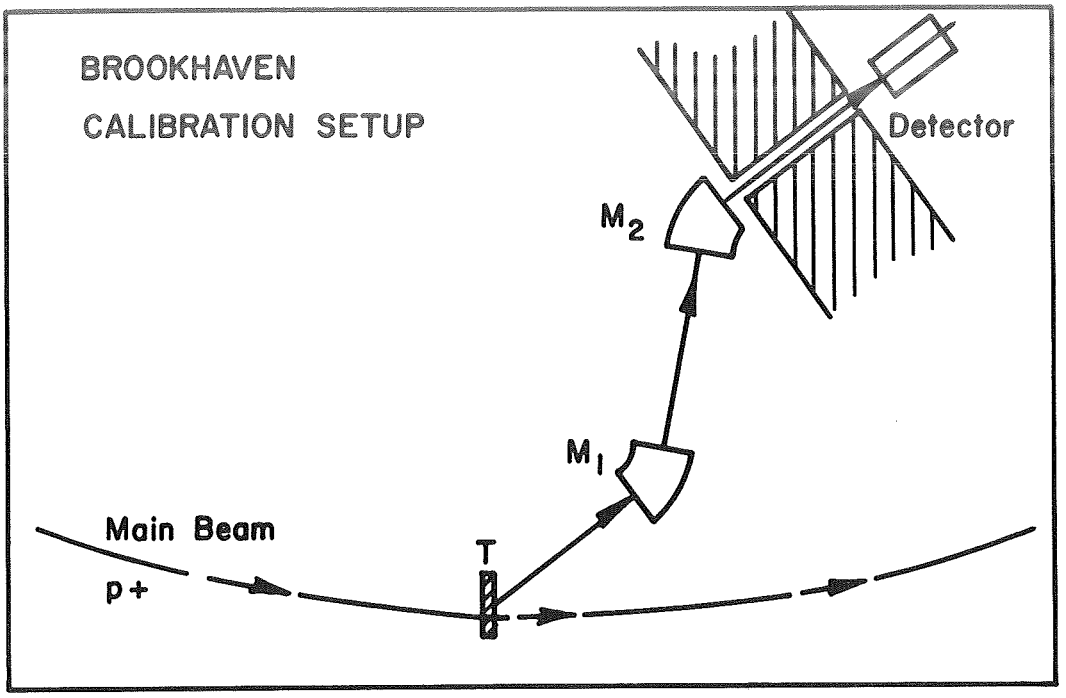
BROOKHAVEN
CALIBRATION SETUP
Detector
M2
M1
Main Beam
p+
T

Fig. 4a

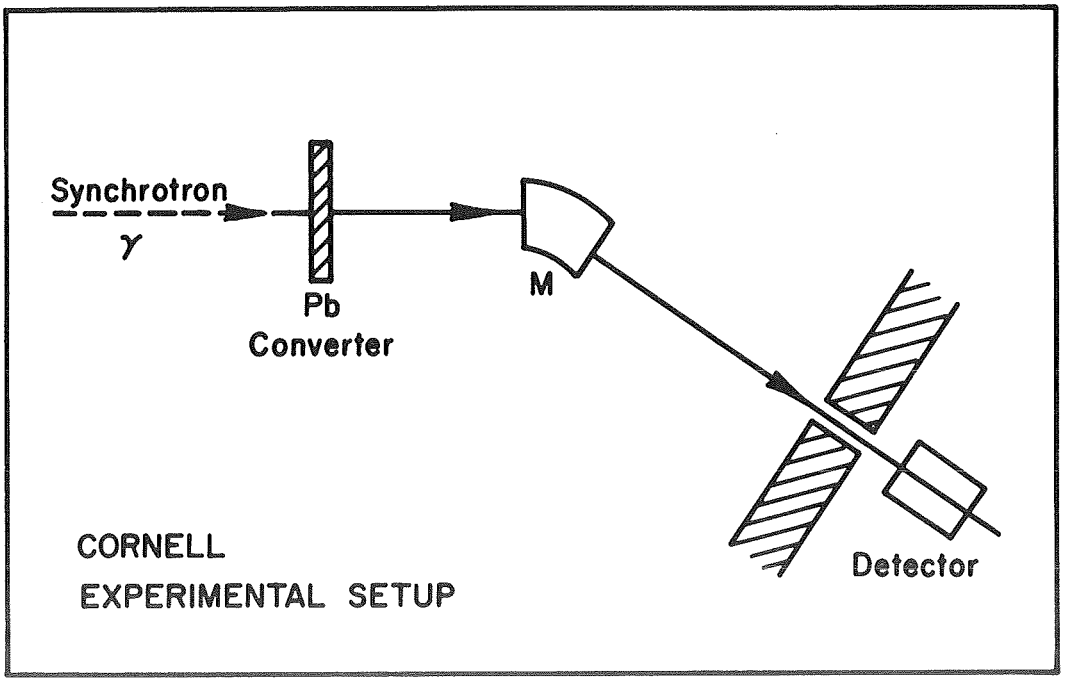
Synchrotron
γ
Pb
Converter
M
Detector
CORNELL
EXPERIMENTAL SETUP

Fig. 4b

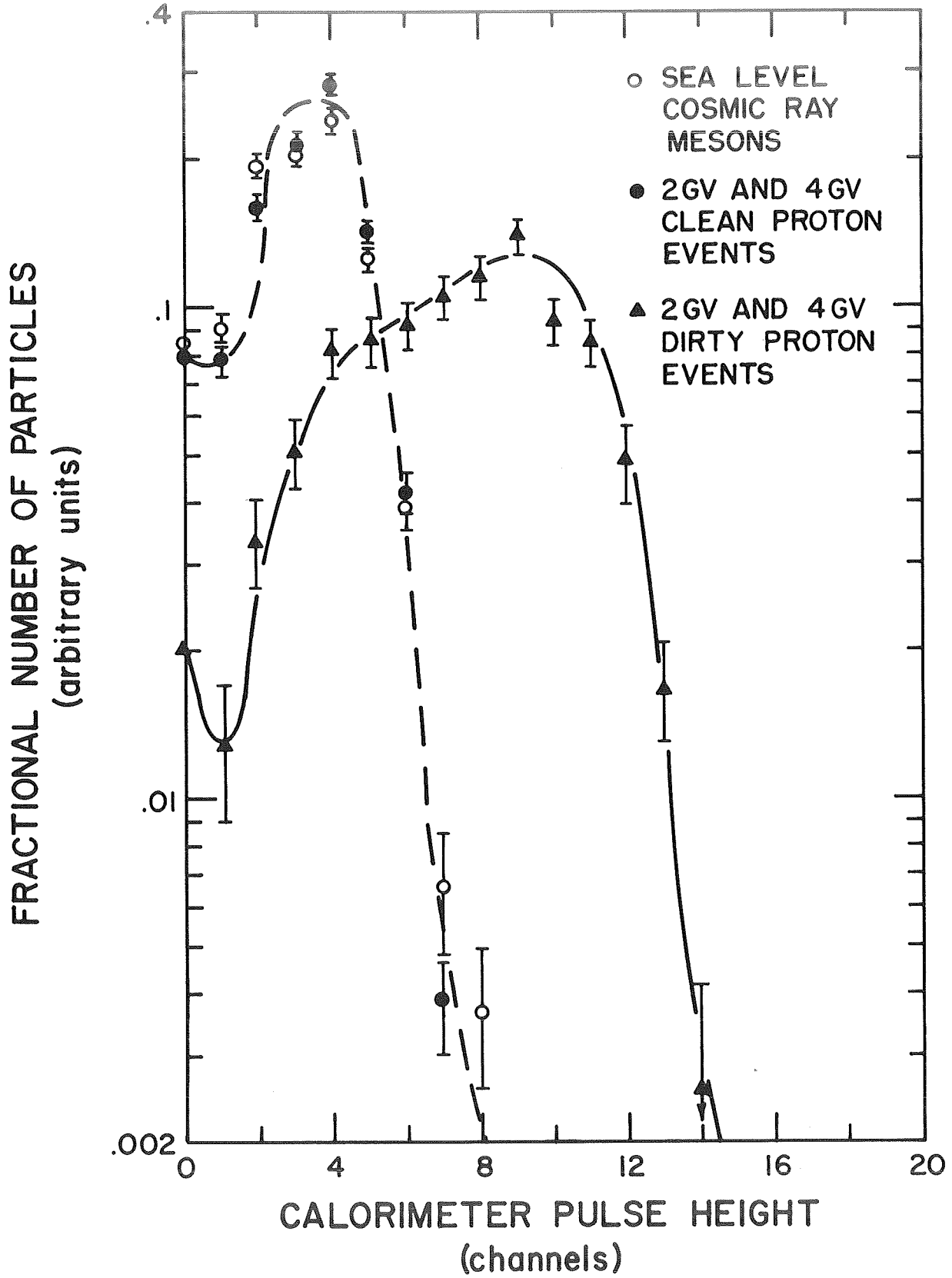
.4
.1
.01
.002
0
4
8
12
16
20
SEA LEVEL COSMIC RAY MESONS
2GV AND 4GV CLEAN PROTON EVENTS
2GV AND 4GV DIRTY PROTON EVENTS
FRACTIONAL NUMBER OF PARTICLES
(arbitrary units)
CALORIMETER PULSE HEIGHT
(channels)

Fig. 5

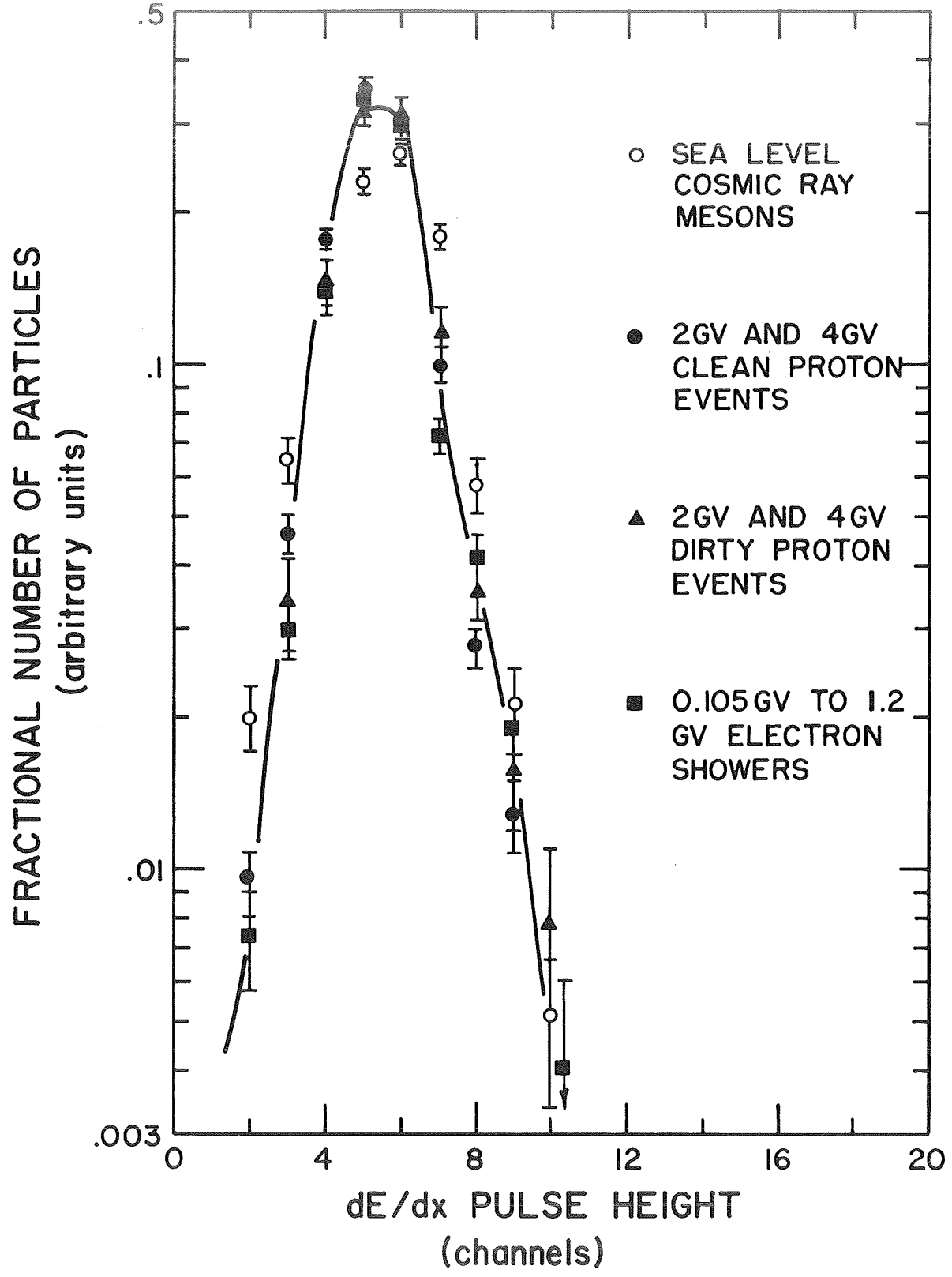
.5
.1
.01
.003
FRACTIONAL NUMBER OF PARTICLES
(arbitrary units)
0
4
8
12
16
20
dE/dx PULSE HEIGHT
(channels)
SEA LEVEL COSMIC RAY MESONS
2GV AND 4GV CLEAN PROTON EVENTS
2GV AND 4GV DIRTY PROTON EVENTS
0.105GV TO 1.2 GV ELECTRON SHOWERS

Fig. 6

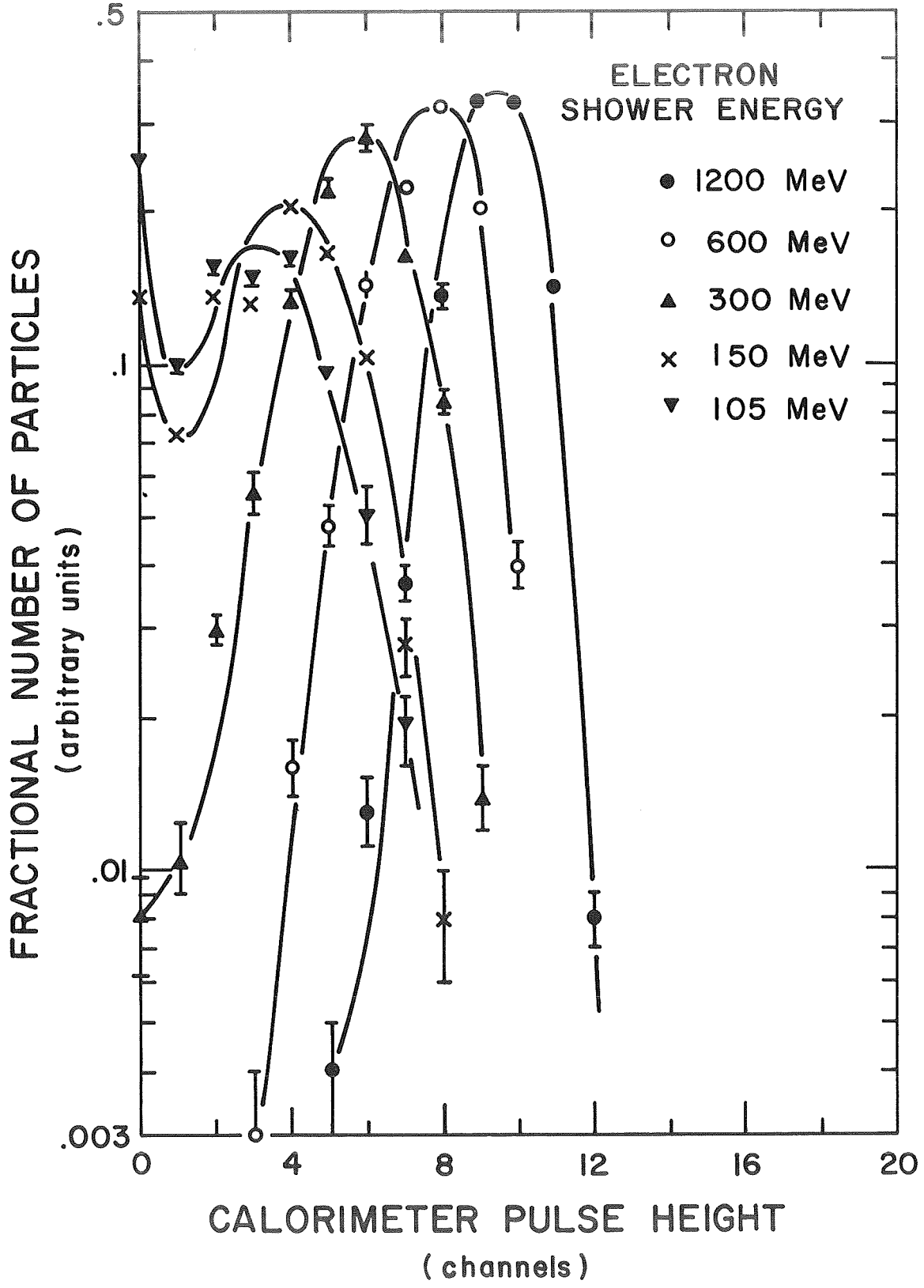
.5
.1
.01
.003
0
4
8
12
16
20
ELECTRON
SHOWER ENERGY
1200 MeV
600 MeV
300 MeV
150 MeV
105 MeV
FRACTIONAL NUMBER OF PARTICLES
(arbitrary units)
CALORIMETER PULSE HEIGHT
(channels)

Fig. 7

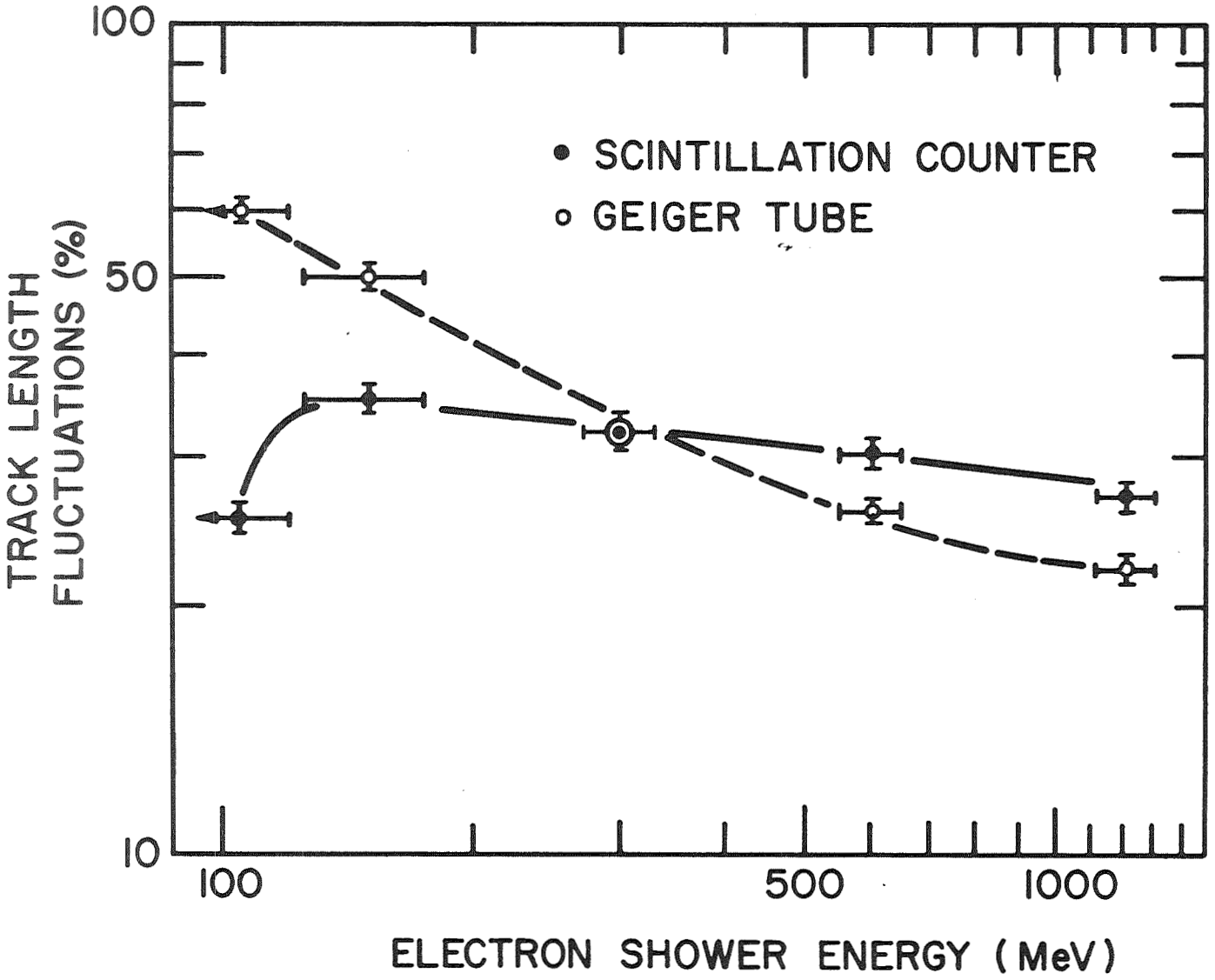
100
50
10
TRACK LENGTH FLUCTUATIONS (%)
• SCINTILLATION COUNTER
o GEIGER TUBE
100
500
1000
ELECTRON SHOWER ENERGY (MeV)

Fig. 8

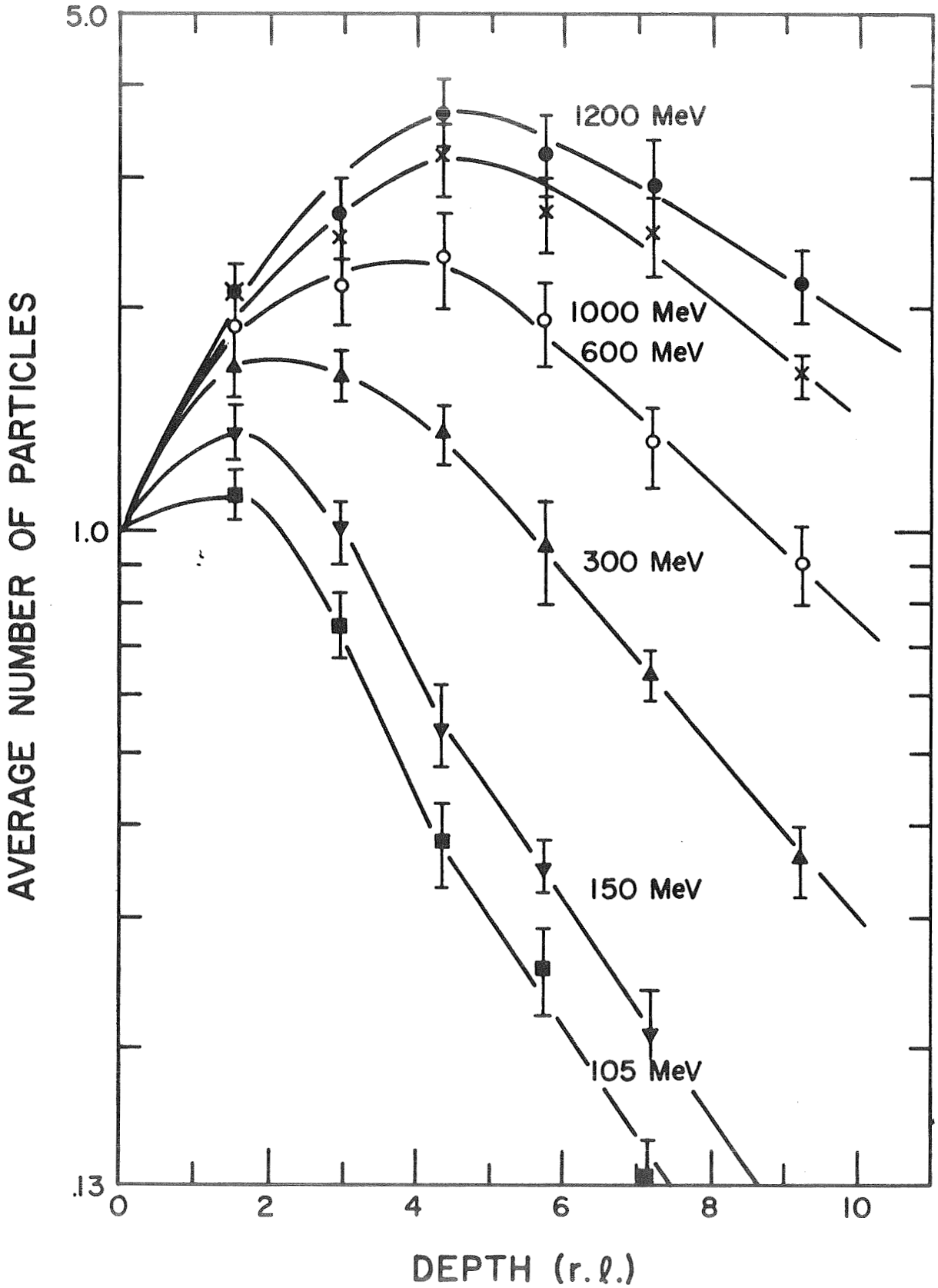
5.0
1.0
.13
AVERAGE NUMBER OF PARTICLES
1200 MeV
1000 MeV
600 MeV
300 MeV
150 MeV
105 MeV
0
2
4
6
8
10
DEPTH (r.ℓ.)

Fig. 9

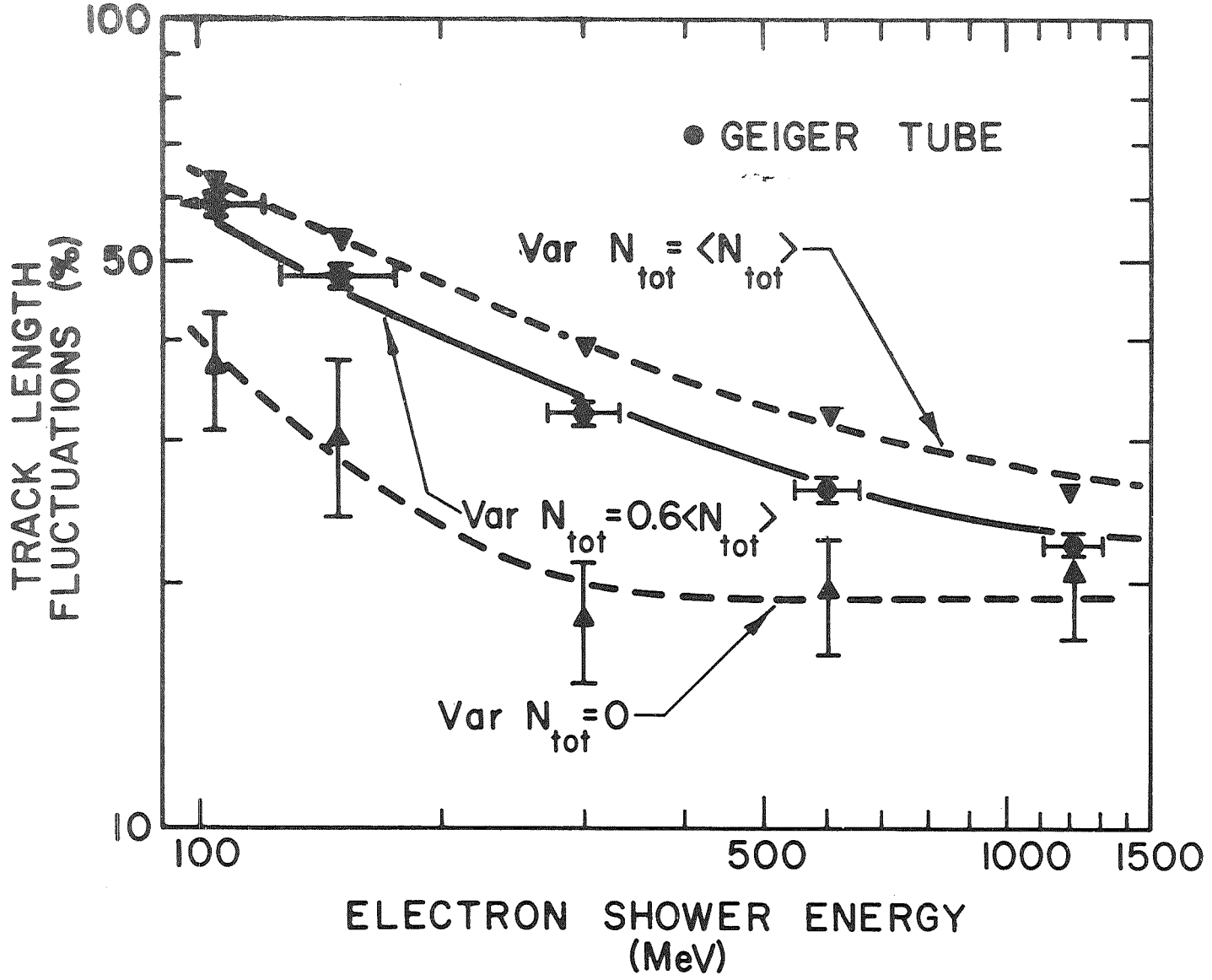
100
50
10
TRACK LENGTH FLUCTUATIONS (%)
● GEIGER TUBE
Var N tot = <N tot>
Var N tot =0.6<N tot>
Var N tot =0
100
500
1000
1500
ELECTRON SHOWER ENERGY (MeV)

Fig. 10

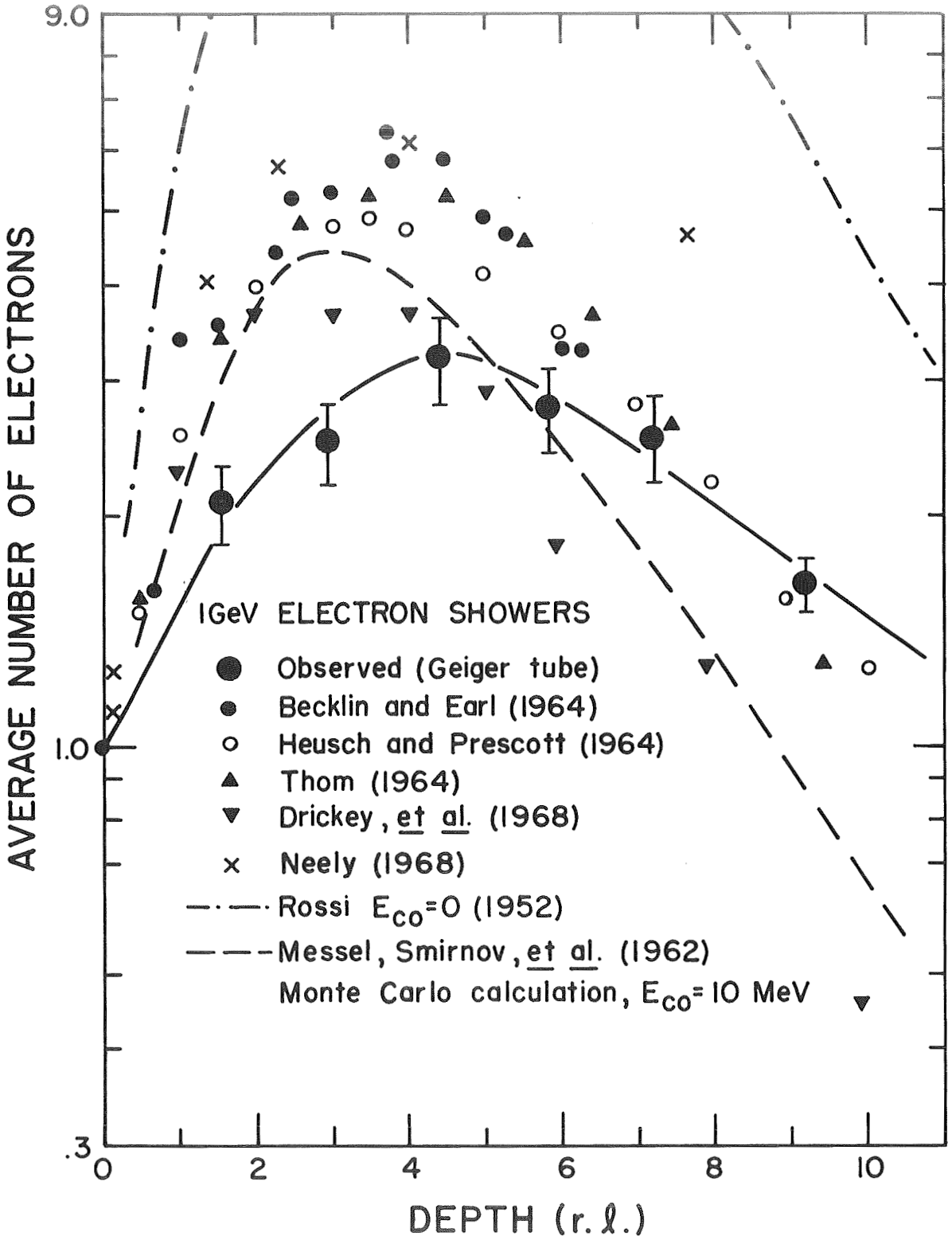
9.0
1.0
.3
AVERAGE NUMBER OF ELECTRONS
0
2
4
6
8
10
DEPTH (r.ℓ.)
1GeV ELECTRON SHOWERS
Observed (Geiger tube)
Becklin and Earl (1964)
Heusch and Prescott (1964)
Thom (1964)
Drickey, et al. (1968)
Neely (1968)
Rossi E_{co}=0 (1952)
Messel, Smirnov, et al. (1962)
Monte Carlo calculation, E_{co}= 10 MeV

Fig. 11

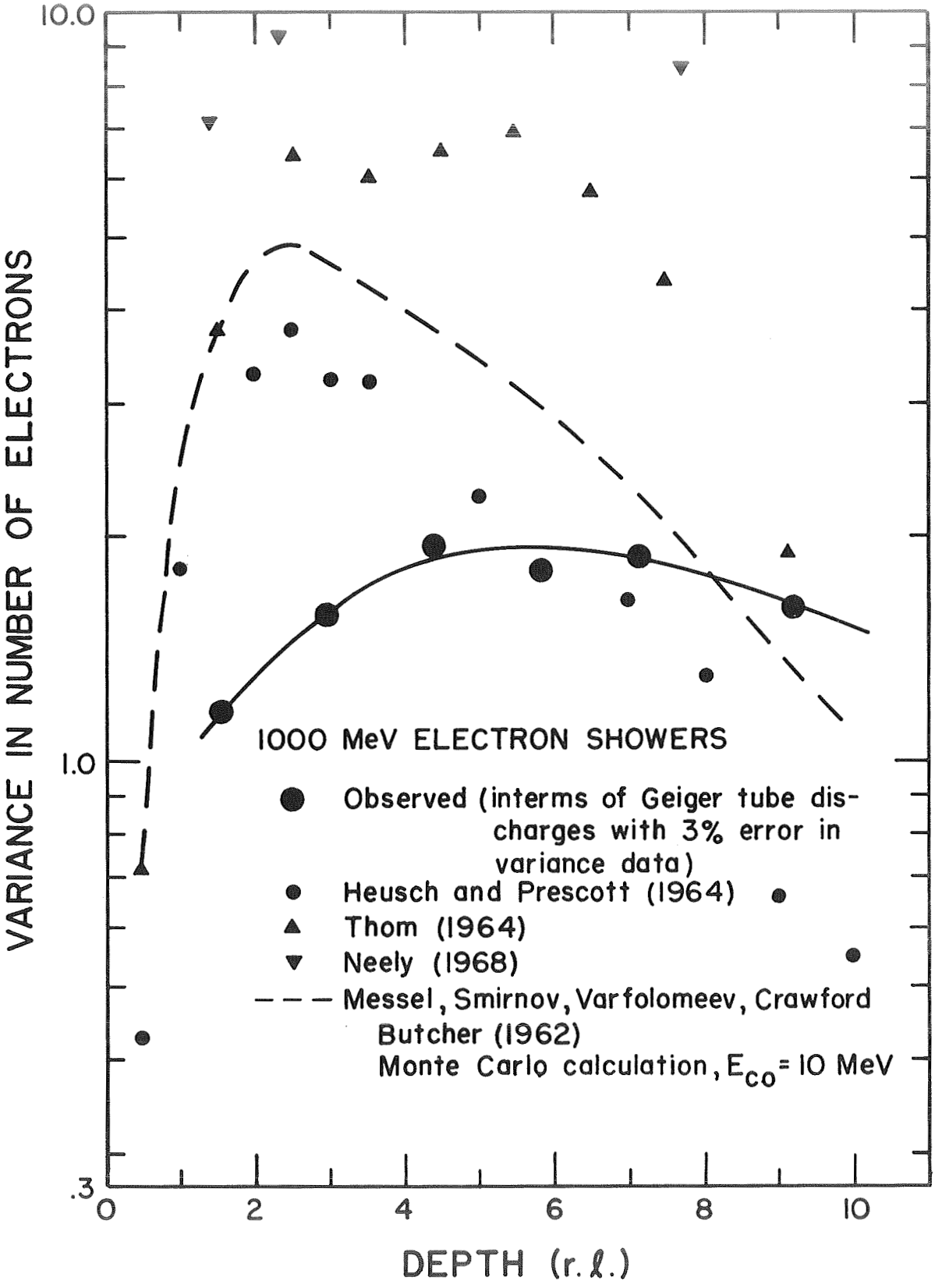
10.0
1.0
.3
VARIANCE IN NUMBER OF ELECTRONS
0
2
4
6
8
10
DEPTH (r.ℓ.)
1000 MeV ELECTRON SHOWERS
Observed (interms of Geiger tube discharges with 3% error in variance data)
Heusch and Prescott (1964)
Thom (1964)
Neely (1968)
Messel, Smirnov, Varfolomeev, Crawford Butcher (1962)
Monte Carlo calculation, E_{co} = 10 MeV

Fig. 12

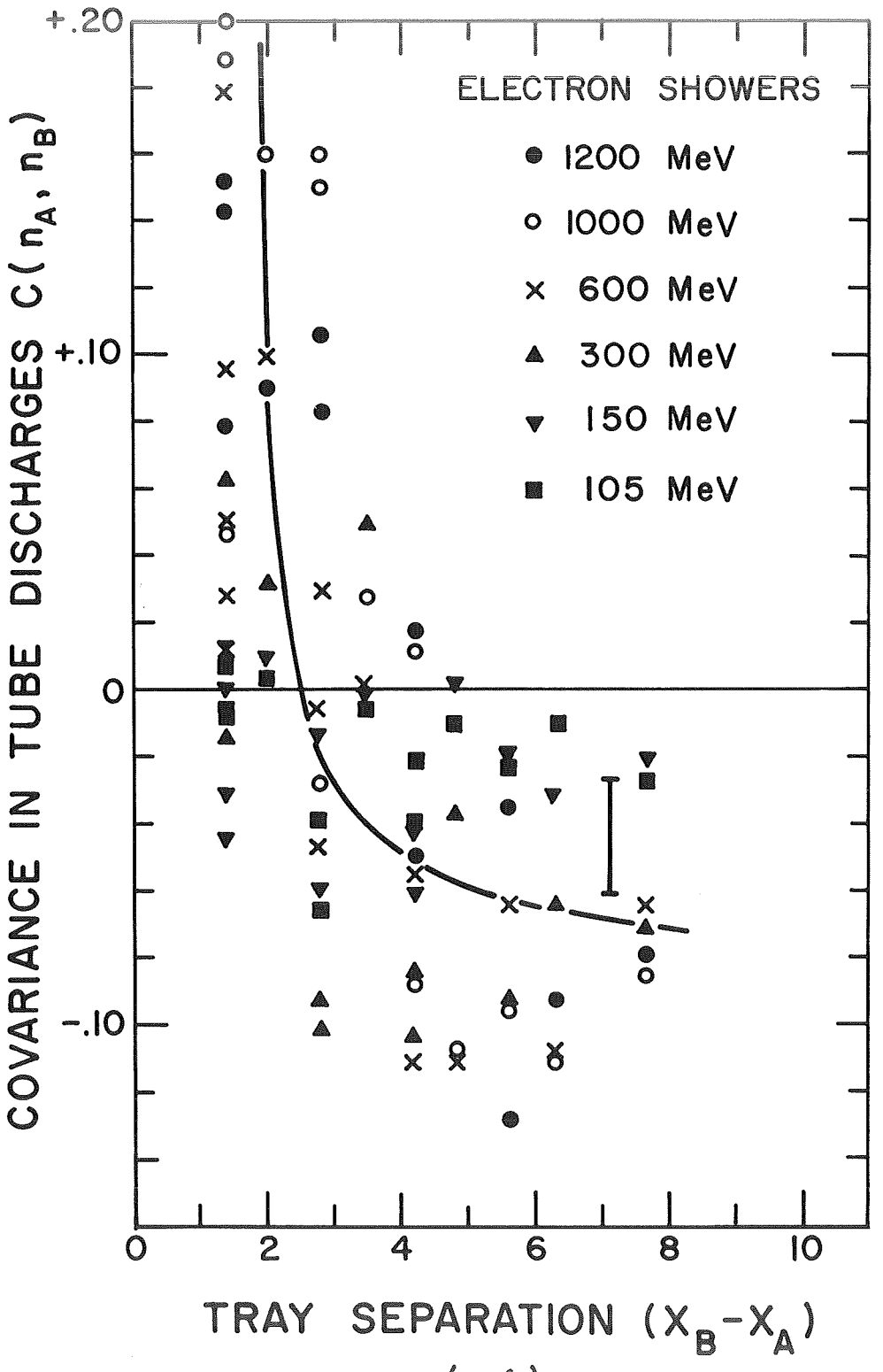
+.20
+.10
0
-.10
ELECTRON SHOWERS
1200 MeV
1000 MeV
600 MeV
300 MeV
150 MeV
105 MeV
COVARIANCE IN TUBE DISCHARGES C(n_A, n_B)
0
2
4
6
8
10
TRAY SEPARATION (X_B - X_A)
(r. ℓ.)

Fig. 13

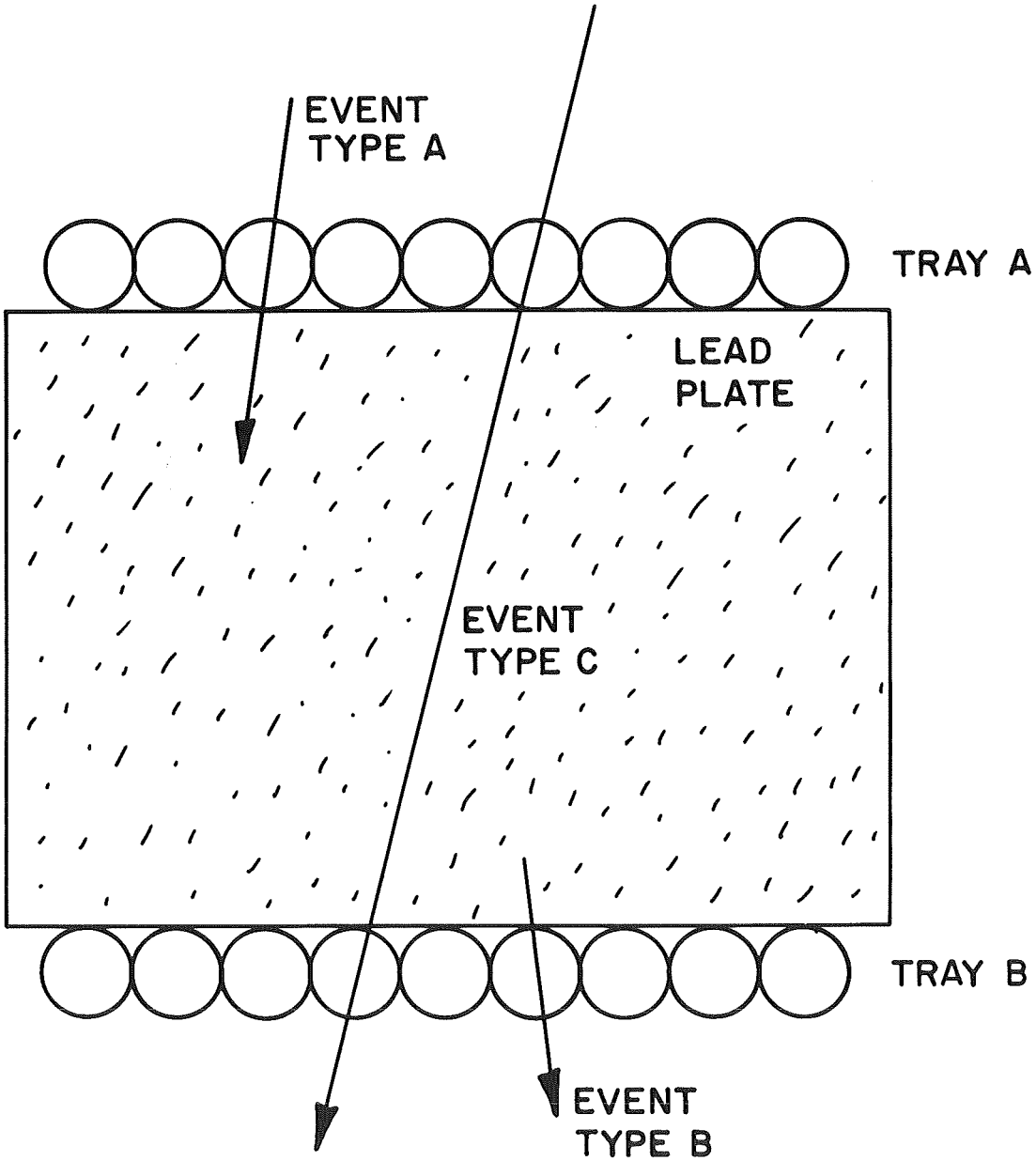

Fig. 14

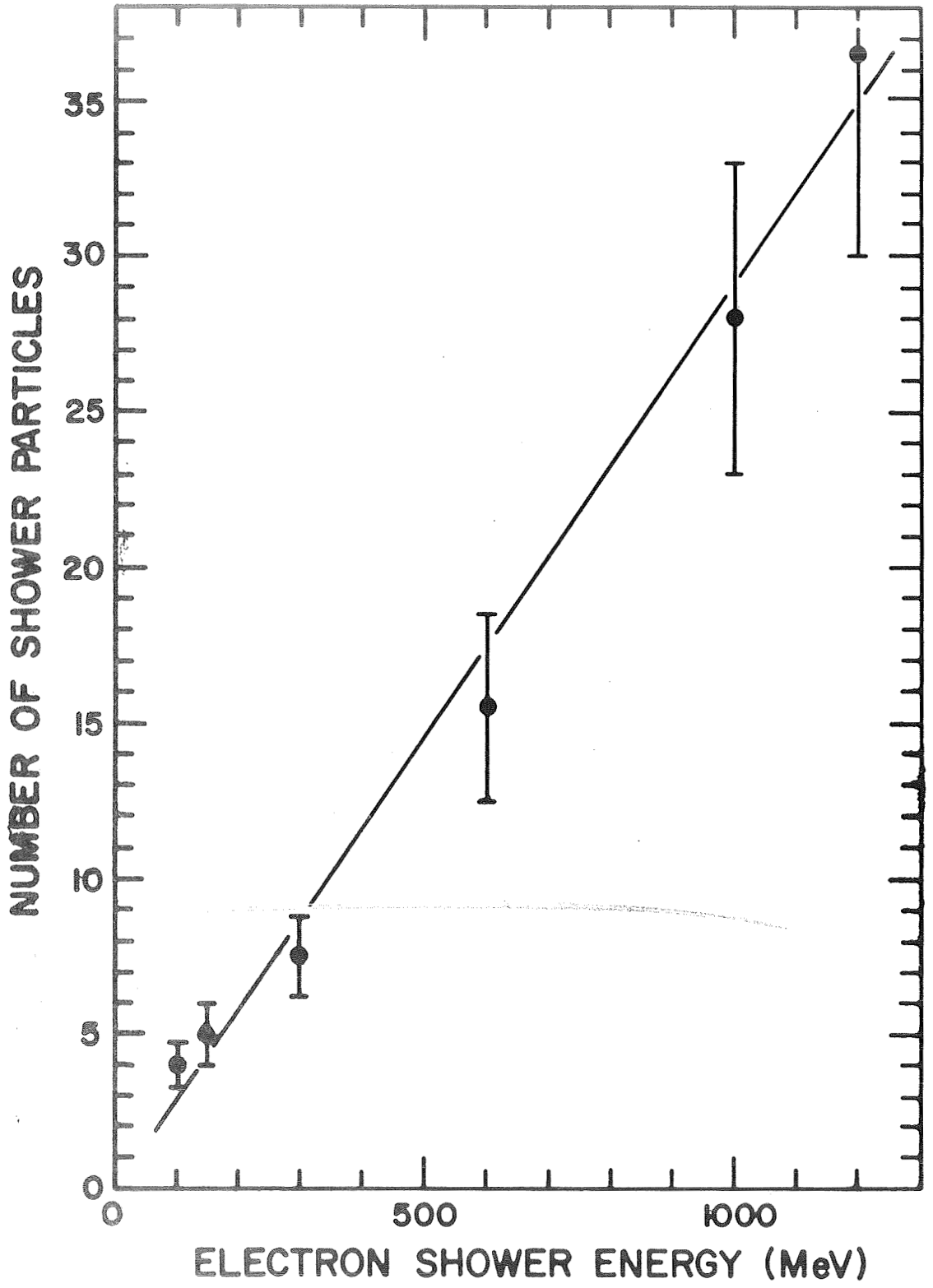
NUMBER OF SHOWER PARTICLES
0
5
10
15
20
25
30
35
0
500
1000
ELECTRON SHOWER ENERGY (MeV)

Fig. 15

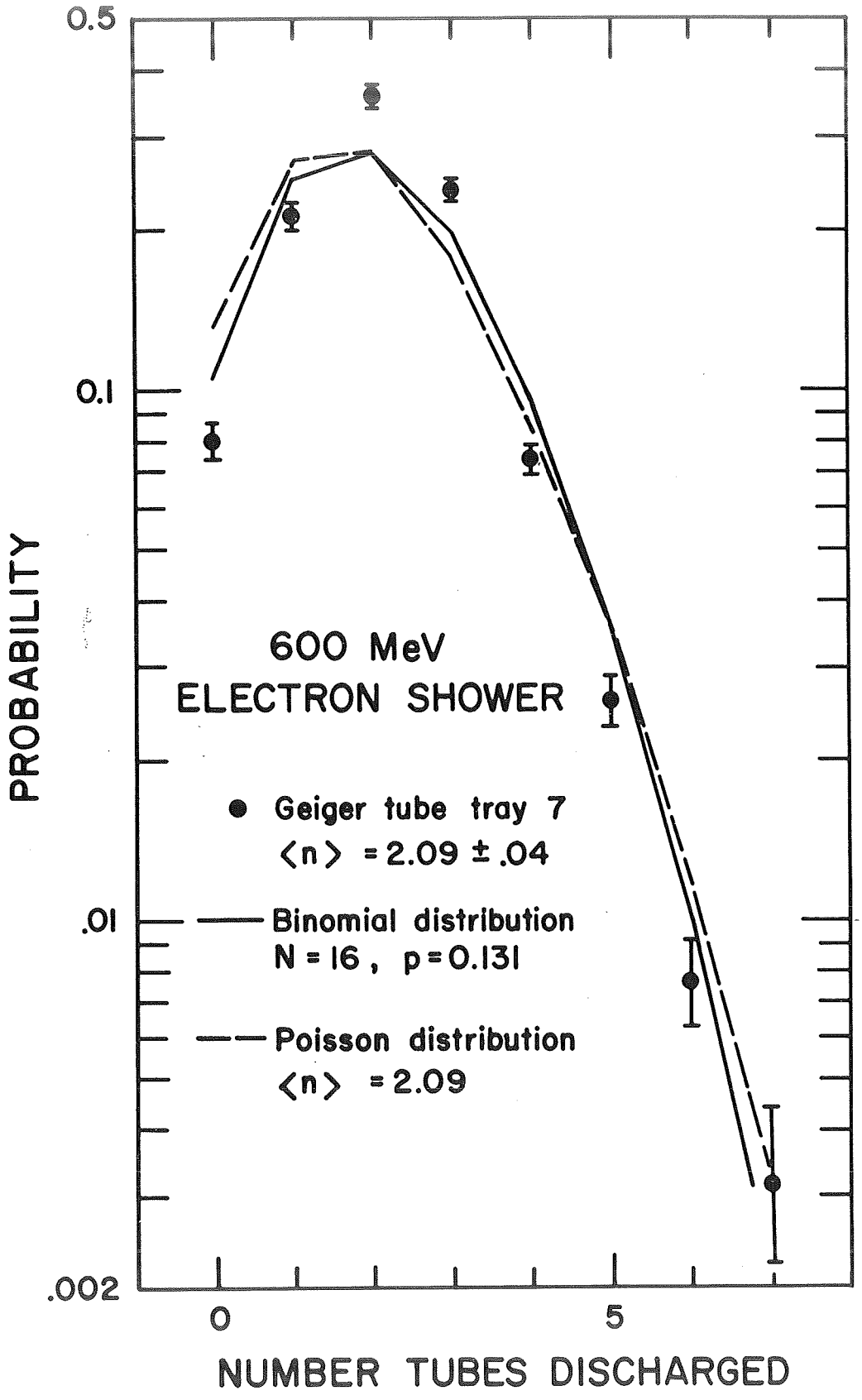
0.5
0.1
.01
.002
PROBABILITY
600 MeV
ELECTRON SHOWER
Geiger tube tray 7
⟨n⟩ = 2.09 ± .04
Binomial distribution
N = 16, p = 0.131
Poisson distribution
⟨n⟩ = 2.09
0
5
NUMBER TUBES DISCHARGED

Fig. 16

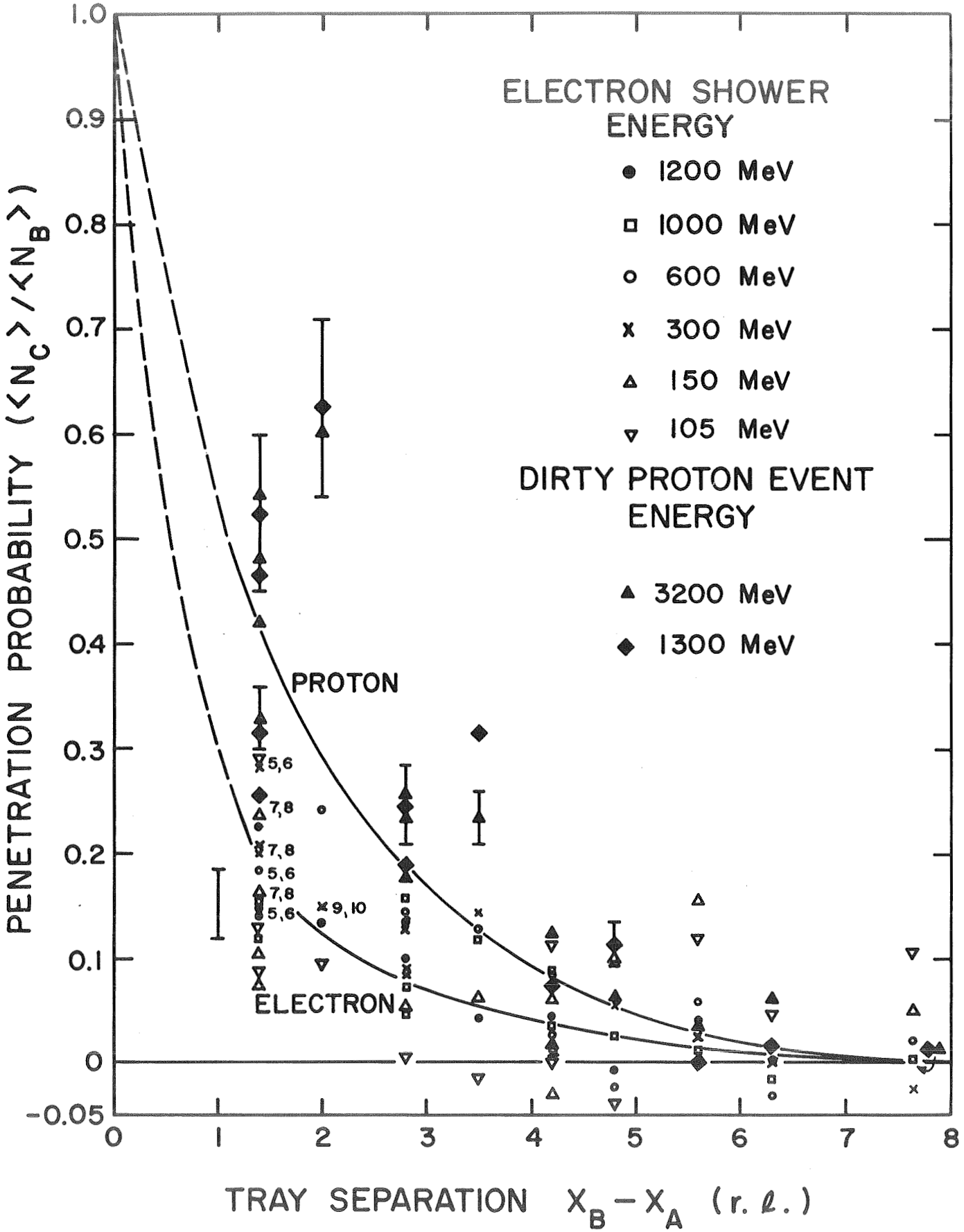
ELECTRON SHOWER ENERGY
1200 MeV
1000 MeV
600 MeV
300 MeV
150 MeV
105 MeV
DIRTY PROTON EVENT ENERGY
3200 MeV
1300 MeV
PROTON
ELECTRON
5,6
7,8
7,8
5,6
7,8
5,6
9,10
PENETRATION PROBABILITY (<N_C>/<N_B>)
TRAY SEPARATION X_B − X_A (r. ℓ.)
1.0
0.9
0.8
0.7
0.6
0.5
0.4
0.3
0.2
0.1
0
-0.05
0
1
2
3
4
5
6
7
8

Fig. 17

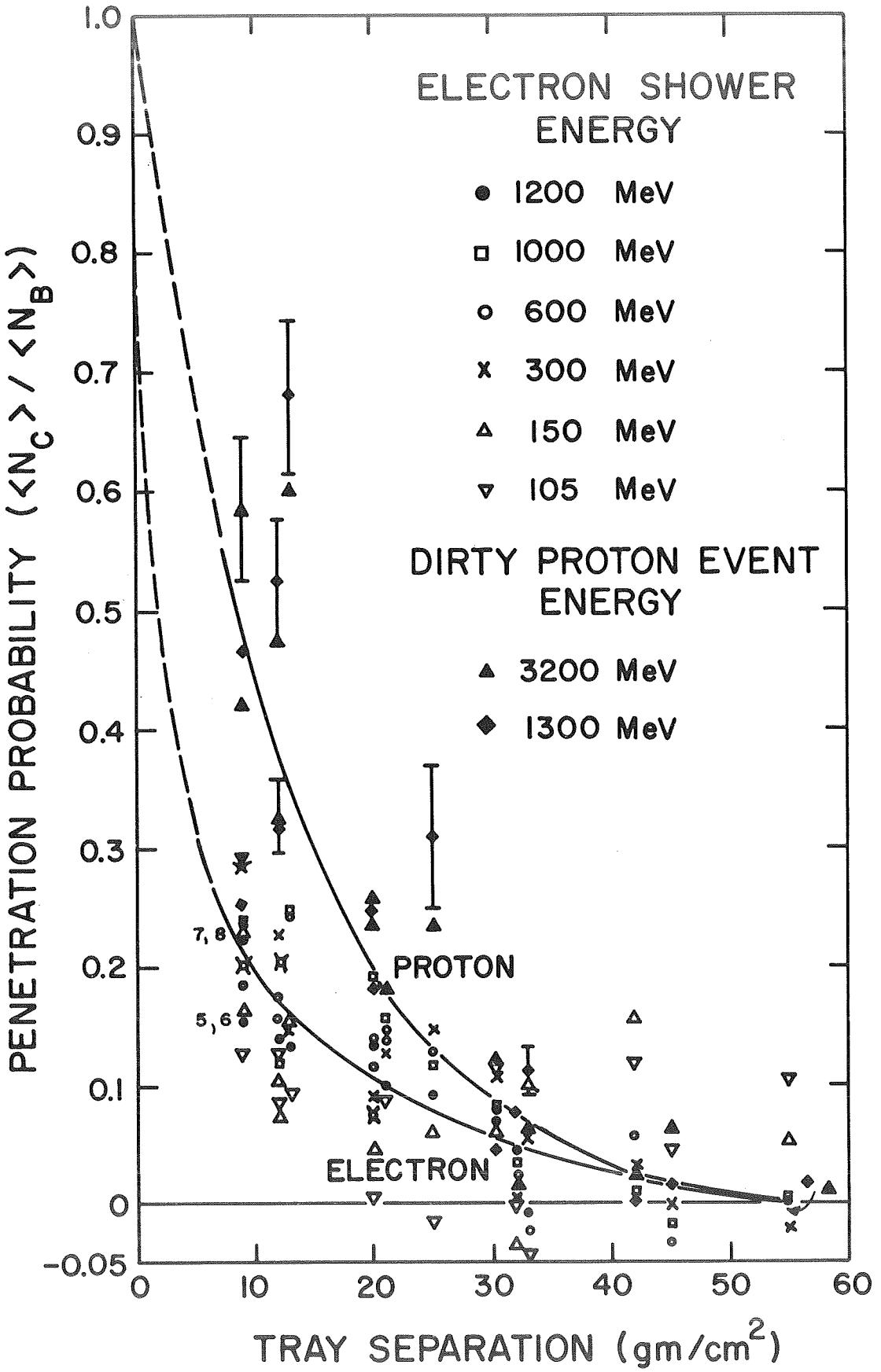
ELECTRON SHOWER ENERGY
1200 MeV
1000 MeV
600 MeV
300 MeV
150 MeV
105 MeV
DIRTY PROTON EVENT ENERGY
3200 MeV
1300 MeV
PROTON
ELECTRON
7,8
5,6
PENETRATION PROBABILITY (<N_C> / <N_B>)
TRAY SEPARATION (gm/cm²)
1.0
0.9
0.8
0.7
0.6
0.5
0.4
0.3
0.2
0.1
0
-0.05
0
10
20
30
40
50
60

Fig. 18